RECENT DEVELOPMENTS IN MODELING, ANALYSIS AND NUMERICS OF FERROMAGNETISM

By

Martin Kružík

and

Andreas Prohl

IMA Preprint Series # 1998

(October 2004)

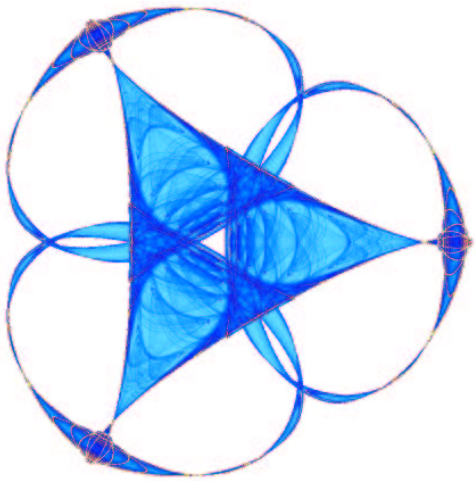

INSTITUTE FOR MATHEMATICS AND ITS APPLICATIONS

UNIVERSITY OF MINNESOTA
514 Vincent Hall
206 Church Street S.E.
Minneapolis, Minnesota 55455–0436

Phone: 612/624- 6066 Fax: 612/626- 7370
URL: http://www.ima.umn.edu

RECENT DEVELOPMENTS IN MODELING, ANALYSIS AND NUMERICS OF FERROMAGNETISM

MARTIN KRUŽÍK AND ANDREAS PROHL

ABSTRACT. Micromagnetics is a continuum variational theory describing magnetization pattern in ferromagnetic media. Its multiscale nature due to different inherent spatio-temporal physical and geometric scales, together with nonlocal phenomena and a nonconvex side-constraint leads to a rich behavior and pattern formation. This variety of effects is also the reason for severe problems in analysis, model validation and reductions, and numerics, which are only accessed recently and are reviewed in this work.

CONTENTS

1. FERROMAGNETISM — A MULTISCALE PROBLEM

Magnetic properties of materials have been known for more than thousand years. About 1000 years back Chinese sailors started to use compasses. Until the 19th century electric and magnetic effects were considered as two independent physical phenomena. In 1820 Oersted proved that an electric current can influence the needle of a compass. Ampere and Faraday explained that behavior and laid the foundation for the unified theory of electrodynamics, which was developed by James C. Maxwell. Since then, permanent magnets have found many applications in energy transforming and data storage devices. In microphones and electric generators they transform the mechanical energy of a membrane or a rotor into electric energy. In loudspeakers and motors the electric energy is transformed back into mechanical energy. Around 1900, Poulsen was the first who recorded an acoustic signal on a ferromagnetic wire opening thus wide applications of magnetic recording. The invention of computers has brought a need of large data storage on easy to handle media. This has led to the fast development of magnetic tapes and floppy disks as well as magnetic hard disks. In general, magnetic media consist of elements, where each of them stores a single bit. The data writing speed is constrained by the magnetization switching time. Therefore, a deeper understanding of magnetization processes and mechanisms is important for the optimal design of magnetic recording media.

Date: October 11, 2004.
1991 *Mathematics Subject Classification.* 49K20, 65K10, 65M12, 65M15, 65N50.
Key words and phrases. Ferromagnet, Landau-Lifshitz, Landau-Lifshitz-Gilbert, mesoscopic, microscopic, harmonic map, nonconvexity, relaxation, numerics.

Ferromagnetic models and simulations can provide reliable information which is experimentally inaccessible at low costs and considerably fast.

The basic idea of micromagnetics is to neglect a quantum-physical description of matter by ignoring its atomic nature and looking at it through the eyes of continuum physics. Such a theory started with the paper by Landau and Lifshitz [68] in 1935 who calculated the structure of a domain wall between two adjacent anti-parallel domains. Later on, William F. Brown [15] developed a theory called micromagnetism. The basic difference to the magnetic domain theory is that one does not describe a shape of a domain in advance and then calculates an optimal magnetic structure but, contrary to that, the domain shape is a subject of optimization.

The theory of rigid ferromagnetic bodies [15, 68] assumes that a magnetization $m : \omega \to \mathbb{R}^n$, which describes the state of a body $\omega \subset \mathbb{R}^n$, $n = 2, 3$, is subjected to the Heisenberg-Weiss constraint, i.e., has a given (in general, temperature dependent) magnitude

$$|\, m \,| = M_{\rm s} \quad \text{almost everywhere in } \omega \ ,$$

where $M_{\rm s} > 0$ is the saturation magnetization. The Helmholtz free energy of a rigid ferromagnetic body $\omega \subset \mathbb{R}^n$ consists of three parts. The first part is the exchange energy, $\alpha \int_\omega |\nabla m|^2 \, {\rm d}x$, $\alpha > 0$ which penalizes spatial changes of m and determines a finest characteristic length scale. The second part is the anisotropy energy $\int_\omega \varphi(m) \, {\rm d}x$ related to crystallographic properties of the ferromagnet. A typical $\varphi : \mathbb{R}^n \to \mathbb{R}^* = \mathbb{R} \cup \{+\infty\}$ is a nonnegative function vanishing only at a few isolated points on S^{n-1} determining directions of easy magnetization, e.g. at two points for uniaxial materials or at six (or eight) for cubic ones. Throughout the paper we will assume that φ is a restriction of a non-negative, even function $\tilde{\varphi} \in C^\infty(\mathbb{R}^n)$ to $S^{n-1} = \{s \in \mathbb{R}^n; |s| \le M_{\rm s}\}$, extended by $+\infty$ out of S^{n-1}, i.e., $\varphi(A) = \tilde{\varphi}(A)$ for $A \in S^{n-1}$ and $\varphi(A) = +\infty$ if $A \notin S^{n-1}$. The third contribution of the Helmholtz energy is the magnetostatic energy $\frac{1}{2} \int_{\mathbb{R}^n} |\nabla u|^2 \, {\rm d}x$, which comes from the stray field $-\nabla u$ governed by

$$\operatorname{div}\big(-\mu_0 \nabla u + m \chi_\omega \big) = 0 \quad \text{in } \mathbb{R}^n \, , \tag{1.1}$$

where $\chi_\omega : \mathbb{R}^n \to \{0, 1\}$ is the characteristic function of ω, and μ_0 is the vacuum permeability. The stray field energy thus penalizes non-divergence free magnetization vectors. Altogether, the Helmholtz energy has the form

$$\alpha \int_\omega |\, \nabla m \,|^2 \, {\rm d}x + \int_\omega \varphi(m) \, {\rm d}x + \frac{1}{2} \int_{\mathbb{R}^n} |\nabla u|^2 \, {\rm d}x \, . \tag{1.2}$$

If the ferromagnetic specimen is exposed to some external magnetic field $H = H(x)$, Zeeman's energy of interactions between this field and magnetization vectors equals $-\int_\omega \langle H, m \rangle_{\mathbb{R}^n} \, {\rm d}x$. Obviously, minimizing Zeeman's energy accounts for aligning m to H. The standard weak formulation of (1.1) implies that the stray field energy can be equivalently expressed as

$$\frac{\mu_0}{2} \int_{\mathbb{R}^n} |\, \nabla u \,|^2 \, {\rm d}x = \frac{1}{2} \int_\omega \langle m, \nabla u \rangle_{\mathbb{R}^n} \, {\rm d}x \, , \tag{1.3}$$

which is more convenient since only the integration over ω is involved.

Remark 1.1. *Suppose $\omega = \mathbb{R}^2 \times (0, \delta)$, for $\delta > 0$. The classical formulation for (1.1) reads*

$$\mu_0 \Delta u = \begin{cases} \operatorname{div} m & \text{in } \mathbb{R}^2 \times (0, \delta) \\ 0 & \text{in } \mathbb{R}^2 \times \big[(-\infty, 0) \cup (\delta, \infty)\big] \end{cases} \ , \quad [u] = 0 \quad \& \quad \mu_0 \big[\frac{\partial u}{\partial x_3} \big] = \mp m_3 \ \text{on } \mathbb{R}^2 \times \{0, \delta\} \, ,$$

where $[\cdot]$ denotes the jump across the boundary of the sample. This implies that there are two sources of stray field, given by the volume charge density $-\operatorname{div} m$ in $\mathbb{R}^2 \times (0, \delta)$ and the surface charge density $\pm m_3$ on $\mathbb{R}^2 \times \{0, \delta\}$.

By accounting to these mechanisms, the Landau energy of the ferromagnet ω for $M_s = 1$, and values $\alpha \ge 0$ reads

$$\mathcal{E}_\alpha(m) = \alpha \int_\omega |\, \nabla m \,|^2 \, {\rm d}x + \int_\omega \varphi(m) \, {\rm d}x + \frac{1}{2} \int_{\mathbb{R}^n} |\, \nabla u \,|^2 \, {\rm d}x - \int_\omega \langle H, m \rangle_{\mathbb{R}^n} \, {\rm d}x \, , \tag{1.4}$$

together with (1.3), for $\mu_0 \equiv 1$. According to Landau's model, observed magnetization patterns correspond to minimizers of this energy; as Brown [15] already outlined, minimizers to (1.4) solve the torque equation that involves the effective field $H_{\text{eff}} = -D\mathcal{E}_\alpha$,

$$m \times H_{\text{eff}} = 0\,.$$

In the sequel, we mainly focus on uniaxial materials (e.g. cobalt) which penalize magnetizations that do not align with the easy axis $e \in \mathbb{R}^n$, i.e., $\varphi(m) = \beta\,|\,\langle m, e_\perp\rangle\,|^2$, $\beta \geq 0$. Media with low value of β are called soft, because the magnetization is easy to rotate. It is the multiscale nature of intrinsic $\alpha, \beta \geq 0$ and geometric scales of the variational problem [33], together with the nonconvex (Heisenberg-Weiss) constraint and nonlocality (stray field contribution) which leads to a rich behavior and pattern formation on intermediate scales.

Historically, physical investigations in micromagnetism initially concentrated on static magnetization configurations observed in bulk specimen up to sub-micrometer size. Early observations of ferromagnetic domains in iron crystals around 1956 revealed both the fascinating intricacies of domain patterns and, nevertheless, their strong geometric nature; decades later, the realm of domain patterns has been enriched by numerous observations, which, in many occasions, have stressed the multiscale nature of their arrangements. One main concept is the competition of wall energy and the energy arising from surface magnetic charges necessarily present in an uniformly magnetized confined specimen. For sizes above the single domain limit, only a finite number of magnetization distributions called (ground) states may be generated, depending on field application and, more generally, magnetic history.

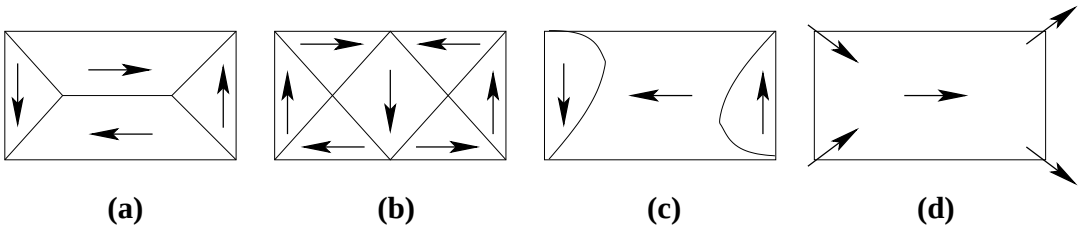

FIGURE 1. Domains: Four different magnetization states in 2 : 1 aspect ratio (cubic) platelets: (a) 'Landau', (b) 'Diamond', (c) 'S', (d) 'Flower'

Observation 1.1. *Computations for Permalloy type materials of size* $2 \times 1\mu m^2$ *for a* $20nm$ *thickness indicate that two flux closure ground states ('Landau' and 'Diamond') have noticeable lower energies than the high remanence states ('S' and 'Flower'), see Figure 1. Intricacies also soon arise when allowing for the existence of complex walls such as cross-tie walls (see Figure 2), which are stable wall structures in continuous Permalloy films in the* $20nm$ *thickness range; for such thicknesses, accurate computations of wall energies prove essential when attempting to define the hierarchy of flux-closure states. As the size decreases to* $0.5 \times 0.25\mu m^2$ *and the thickness to* $10nm$*, however, then the 'Landau' state becomes the lowest energy state and, soon followed, however, by the 'S' state, the 'Diamond' state and, last, the 'Flower' state. Clearly, the 'Flower' state is closest to an uniformly magnetized state. However, the 'S' state appears only marginally metastable and, besides, may easily be generated through the application of the saturating field at an angle to the horizontal axis. These considerations show that submicron dimensions need to be reached before high-remanence states, i.e., the states proper to memory applications for instance, may be considered sufficiently stable. As easily guessed from purely magnetostatic arguments, platelet properties exhibit a strong shape dependence, leading even to configurational anisotropy for platelets with high symmetry, such as squares, triangles, or pentagons, where the conventional shape anisotropy vanishes.*

Domains of ground states are separated by interfaces called walls which exhibit internal structure and are of order $\mathcal{O}(\sqrt{\frac{\alpha}{\beta}})$ thick, which typically amounts to a few dozens of nanometers. According to their structure, different simple (Bloch, Néel walls) and complex walls (cross-tie walls, asymmetric Bloch and Néel walls) are known [51]; see Figure 2. Structures of even smaller size are vortices in thin films and Bloch lines in bulk

materials. Vortices appear as embedded structures in cross-tie walls or at the intersection of domain walls, leading do nontrivial topological arrangement of the magnetization field. Their dynamics is highly nontrivial and at the present time poorly understood.

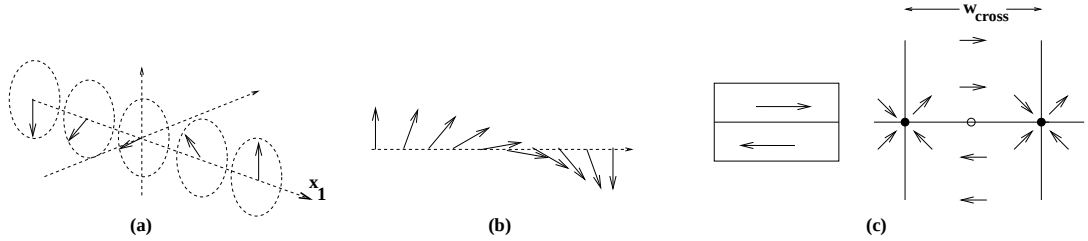

FIGURE 2. Domain walls: (a) Bloch wall, (b) Neel walls (simple walls), (c) Cross-tie wall (complex wall): mesoscopic (left) and microscopic (right) structure

Observation 1.2. *Domain walls are transition layers between magnetic domains which possess a rich internal structure. The simplest among them are 180 degree plane walls separating two domains of opposite direction: The Bloch wall (Figure 2 (a)) occurs in bulk materials, where transition proceeds perpendicular to the transition axis; the main feature of this scenario is avoidance of magnetic volume charges, i.e.,* $\operatorname{div} m = 0$. *If rotation proceeds in the plane spanned by the transition axis and end states, this layer is referred to as Néel wall (Figure 2 (b)). It is the dominating type of wall in very thin films, where Bloch walls would create significant surface charges; Néel walls completely avoid surface charges, but are source of (small) out-of plane magnetization, as well as volume charges. In moderately thick films the most common wall type is the cross-tie wall (Figure 2 (c)). This energetically more favorable composite wall replaces the 180 degree Néel wall by a pattern of a main Néel-wall segment (orientationally favored by the anisotropy energy) and perpendicular short Néel wall segments (the 'cross-ties') periodically lining up at a new scale* w_{cross}. *All Néel walls in the cross-tie pattern show transition angles of 90 degrees or less.*

Besides multiple spatial scales, micromagnetism shows a rich variety of complex nonstationary phenomena; historically, the study of magnetization reversal processes in the quasi-static regime came first, where the spin configuration is observed following the magnetization loop of an applied field. In contrast to static and quasi-static investigations, the wide variety of dynamic properties of magnetic elements can only be understood by precessional motion to explain spin dynamics and switching dynamics at speeds of pico- or even femptosecond timescales; cf. Figure 3. Mesoscopic changes during a corresponding experiment may be displayed by hysteresis loops, which plot the average magnetization at the steady state as a function of the applied field strength; see Figures 3 (d), 15.

Observation 1.3. *If we apply an external magnetic field to a (fully demagnetized) ferromagnet, the ferromagnet absorbs part of the external field by growing aligned domains until saturation is reached. Even when the external field is removed, the magnet will retain some field (remancence): it has become magnetized. See e.g. Figure 3 (d). When the external field is cycled in time the corresponding magnetization of the magnet traces a hysteresis loop. In many cases we observe that the dependence of the magnetization on the external field is rate-independent, which means that it is invariant to any increasing time homeomorphism. The property of rate-independence is named after Truesdell and Noll* [96]. *Following Visintin* [98], *we define hysteresis as a rate-independent memory effect. Actually, typical memory effects in ferromagnetism are not purely rate-independent, since hysteresis is coupled with viscous effects. However, rate-independence prevails provided that the evolution is not too fast. See e.g .* [99] *for a version of Landau-Lifshitz equation accounting for rate-independent effects.*

The interest in magnetic materials obtained a completely new and unforeseen momentum when growth and lithographic patterning methods, known from the field of semiconductors, were applied to magnetic material classes, which resulted in the discovery of a number of fascinating properties: starting with the growth of artificial layered magnetic materials, with layer thicknesses on the atomic scale, the giant magnetoresistance effect and quantum size effects in the electronic and magneto-optical properties have been seen.

These studies pose new questions, for example about the magnetization reversal process induced by external field pulses of short duration, the role of precessional damping, nonstationary magnetization patterns and magnetic anisotropies, as well as the influence of geometric shape and size of ferromagnetic specimen in this field-induced reversal process. For example, the dynamics of small magnetic elements is expected to differ from that measured in (single-layer) magnetic films due to different relative roles played by exchange and anisotropy energy contributions driving the evolution.

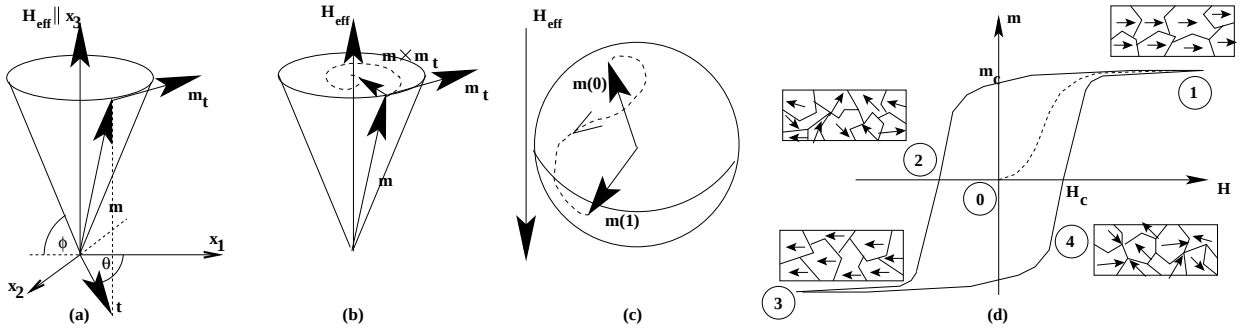

FIGURE 3. Magnetization precession (a) without damping, (b) with damping; (c) switching/reversal process; (d) virgin curve and hysteresis loop

Mathematical models in ferromagnetism focus on certain ranges of spatio-temporal scales to describe corresponding magnetic phenomena. The following levels of description may be distinguished:

(1) *Atomic level*: statistical physics is used to describe single magnetic spin moments and their interaction in a finite ensemble.
(2) *Microscopic level*: continuum physics is used to describe the problem. Usually scales about 1 μm down to dozens of nanometers can be treated. The commonly used models at this level are the nonconvex, nonlocal Landau-Lifshitz energy functional and the strongly coupled, degenerated quasilinear parabolic Landau-Lifshitz-Gilbert equation e.g. to predict structure and evolution of domains and walls. See Sections 2.2, 3.2.
(3) *Mesoscopic level*: characteristic microscopic length scales of the magnetic material are ignored in a large body limit to model specimen of engineering interest. The averaged magnetization is a global minimizer of a degenerate convex, nonlocal, asymptotic variational problem, and microstructure is described by volume fractions of particular magnetic poles. Further applications include description of inhomogeneous magnetization in bulk specimen up to millimeter size and microstructure in single crystals; cf. Sections 2.3, 3.3.
(4) *Macroscopic level*: Information about microstructure is suppressed, and phenomenological constitutive laws describe evolution of gross magnetization during external loading. This simplification compromises level (3) with high-performance computational realizability needed for advanced applications.

Over the last decades, considerable effort has been made to study mathematically related stationary and nonstationary models for different regimes of scales: next to well-posedness and further characterizations of solutions (e.g., study of singularity sets, asymptotics), models have been validated through theoretical predictions (e.g., prediction of phenomena, scaling laws, reduced models). Mathematical difficulties inherent to these models (e.g., nonconvexity, nonlocality, strong nonlinearities, degeneracies, measure valued solutions) as well as multiple scales inherent to solutions also make the construction of efficient, convergent numerical schemes a nontrivial task. The goal of this article is to survey recent status in mathematical modeling, analysis, and numerics of ferromagnetism as it appears to the authors.In the sequel, we are going to use standard Lebesgue spaces L^p, Sobolev spaces H^1, or spaces of bounded variations BV.

2. Stationary models — multiscale properties of ground-state magnetizations

The variational theory of Landau and Lifshitz [68] describes magnetizations and corresponding domain-wall structures inside a ferromagnetic body $\omega \subset \mathbb{R}^n$ as minima of the energy functional

$$\mathcal{E}_\alpha : \mathcal{A} \cap H^1(\omega, \mathbb{R}^n) \to \mathbb{R}\,, \qquad \mathcal{A} = \Big\{ \phi \in L^2(\omega, \mathbb{R}^n) \Big| \; |\,\phi\,| = 1 \text{ a.e. in } \omega \Big\}\,,$$

given in (1.4). The anisotropy density $\varphi \geq 0$ is zero in case $m \parallel e_i \in \mathbb{R}^n$, for $i \in I$, with some index set I, and positive else. Vectors $e_i \in \mathbb{R}^n$ are referred to as easy axes. The model describes multiscale domain branching and structured domain walls by competition of local and nonlocal energy contributions in (1.4), which are observed in experiments for ferromagnets of different anisotropic materials (e.g. uniaxial, where $\#I = 1$, or cubic, where $\#I = 3$ or 4): for example,

(1) multiscale branching near surfaces in uniaxial materials is explained by reduced magnetostatic energy contributions which only depend on the domain width of the last branching generation at the boundary $\partial\omega$.

(2) geometric structure of domain walls may be explained by accounting to competing effects due to all involved energy contributions.

As can be easily deduced from harmonic mapping theory [52, 92], solutions $(\,m, u\,) \in \mathcal{A} \times H^1(\mathbb{R}^n)$ to (1.4) exist and may be characterized in terms of regularity, provided that $\alpha > 0$; a nontrivial task due to the nonconvex side-constraint is to construct a stable numerical scheme for restricted (finite element) functions to approximate solutions to (1.4), (1.1); see Section 2.2.

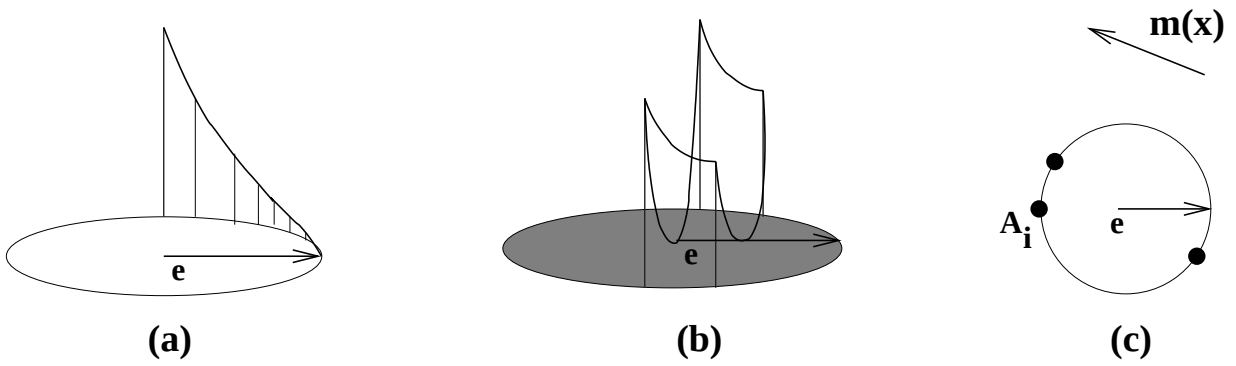

Figure 4. Minimization of Landau-Lifshitz energy: (a) direct minimization: $m(x) \in S^{n-1}$, (b) convexification: $|\,m(x)\,| \leq 1$, (c) Young-measure relaxation: $\nu_x = \sum_{i=1}^{3} \alpha_i \delta_{A_i}$ (example)

The model of Landau and Lifshitz describes equilibria for ferromagnetic bodies on a microscopic level; in contrast, mesoscopic models are in demand for practical applications to describe averaged magnetizations for bulk specimen typically of millimeter-size. This goal motivates a reduced version of (1.4) which is obtained by deleting the exchange energy contribution, i.e., if $\alpha = 0$,

$$\mathcal{E}_0 : \mathcal{A} \to \mathbb{R}\,, \tag{2.1}$$

allowing for infinite variations (microstructure) in space; proper mathematical objects to describe minimizing magnetization configurations of a relaxed version of this energy functional are Young measure solutions. We refer to [81, 89] for detailed expository on Young measures and applications. The Young measure $\nu = \{\nu_x\}_{x\in\omega} \in L^\infty_{\mathrm{w}}\big(\omega, \mathcal{M}(S^{n-1})\big)$, $\|\nu_x\| = 1$, for almost all $x \in \omega$, and where $\mathcal{M}(S^{n-1})$ denotes measures supported on S^{n-1}. Here the subscript "w" means weakly measurable maps, i.e. $x \mapsto \int_{S^{n-1}} f(A)\nu_x(\mathrm{d}A)$ is measurable for any f continuous on S^{n-1}. Young measures encode (oscillatory) microstructures and also allow for calculation of averaged magnetizations $m(x) = \int_{S^{n-1}} A\nu_x(\mathrm{d}A)$, with $|\,m(x)\,| \leq 1$, for almost every $x \in \omega$. The relaxation of $\mathcal{E}_0 : \mathcal{A} \to \mathbb{R}$ for the proper compact convexification

$$\overline{\mathcal{A}} = \Big\{ \nu = \{\nu_x\}_{x\in\omega} \Big|\; \operatorname{supp}\nu_x = S^{n-1},\; x \mapsto \nu_x \text{ weakly measurable} \Big\}$$

of $\mathcal{A}$ in $L^1\big(\omega; C(S^{n-1})\big)^* = L^\infty_{\mathrm{w}}\big(\omega; \mathcal{M}(S^{n-1})\big)$ asks for minima of $\overline{\mathcal{E}_0} : \overline{\mathcal{A}} \times L^2(\omega;\mathbb{R}^n) \to \mathbb{R}$, where

$$\begin{aligned} &\overline{\mathcal{E}_0}(\nu) := \textstyle\int_\omega \int_{S^{n-1}} \varphi(A)\nu_x(\mathrm{d}A)\,\mathrm{d}x + \frac{1}{2}\int_{\mathbb{R}^n} |\,\nabla u\,|^2\,\mathrm{d}x - \int_\omega \langle H, m\rangle_{\mathbb{R}^n}\,\mathrm{d}x\,, \\ &\text{subject to} \qquad m(x) = \textstyle\int_{S^{n-1}} A\nu_x(\mathrm{d}A) \quad \text{and} \quad \Delta u = \mathrm{div}(\chi_\omega m) \quad \text{in } \mathbb{R}^n\,. \end{aligned} \tag{2.2}$$

Minimization of (2.1) and (2.2) are linked together by standard relaxation theory, i.e., (i) $\inf_{\mathcal{A}} \mathcal{E}_0 = \min_{\overline{\mathcal{A}}} \overline{\mathcal{E}_0}$, (ii) minimizers of $\overline{\mathcal{E}_0}$ are weak limits of minimizing (sub-)sequences of $\mathcal{E}_0$, and (iii) minimizing (sub-)sequences of $\mathcal{E}_0$ weakly tend to minimizers of $\overline{\mathcal{E}_0}$. It is nontrivial to ensure that the magnetostatic energy in (2.2) evaluated along a minimizing sequence of (1.4) converges to the weak limit of a minimizing sequence for (1.4). The basic tool to show that is the Div-Curl Lemma [79, 95]. Indeed, as $m_k \to m$ weakly* in $L^\infty(\omega,\mathbb{R}^n)$, $\nabla u_k \to \nabla u$ weakly in $L^2(\mathbb{R}^n,\mathbb{R}^n)$, and since $\{\nabla u_k\}$ is curl-free it is sufficient to show that $\{\mathrm{div}\, m_k\}$ is compact in $H^{-1}_{\mathrm{loc}}(\mathbb{R}^n)$. Then we have

$$\int_\omega \langle m_k, \nabla u_k\rangle_{\mathbb{R}^n}\,\mathrm{d}x \to \int_\omega \langle m, \nabla u\rangle_{\mathbb{R}^n}\,\mathrm{d}x\,.$$

Therefore, it would be natural to define measure valued magnetization as Young measure supported on S^{n-1} which is generated by sequences $\{m_k\}$, where $\{\mathrm{div}\, m_k\} \Subset H^{-1}_{\mathrm{loc}}(\mathbb{R}^n)$. This would impose an additional constraint on the Young measure. Fortunately, as shown in [32, 80, 81], any Young measure supported on S^{n-1} can be generated by a sequence satisfying the compactness constraint.

We now briefly explain the construction in $\mathbb{R}^2$ which was already used in [32]. Suppose that $A_1, A_2, A_3 \in S^{n-1}$ support the Young measure solution $\nu = \vartheta\mu\delta_{A_1} + \vartheta(1-\mu)\delta_{A_2} + (1-\vartheta)\delta_{A_3}$ (Note that $n+1$ points are sufficient in n dimensions). Any $m^k \in L^2(\omega;\mathbb{R}^2)$ can be approximated by piecewise constant functions on ω. Thus the problem turns into an approximation of a constant function on a given set $O \subset \omega$. Take $q \in \mathbb{R}^2$, such that $\langle \mu A_1 + (1-\mu)A_2 - A_3, q\rangle_{\mathbb{R}^2} = 0$, and $p \in \mathbb{R}^2$ in such way that $\langle A_1 - A_2, p\rangle_{\mathbb{R}^2} = 0$. This choice of p, q ensures the convergence of magnetostatic energies. Define

$$\theta(t) = \begin{cases} 1 & \text{if } 0 \le t < \vartheta \\ -1 & \text{if } \vartheta \le t < 1 \end{cases} \quad \text{and} \quad \eta(t) = \begin{cases} 1 & \text{if } 0 \le t < \mu \\ -1 & \text{if } \mu \le t < 1 \end{cases}$$

and extend them periodically over the whole space. Then we define for $\xi, \zeta \in \mathbb{N}$

$$\mathcal{L}_{\xi\pm} = \{x \in O;\ \theta(\xi\langle x, q\rangle_{\mathbb{R}^2}) = \pm 1\}\,, \qquad \mathcal{M}_{\zeta\pm} = \{x \in O;\ \eta(\zeta\langle x, p\rangle_{\mathbb{R}^2}) = \pm 1\} \cap \mathcal{L}_{\xi+}\,.$$

Then we have

$$\tilde{m}_{\xi,\zeta}(x) = \begin{cases} A_1 & \text{if } x \in \mathcal{M}_{\zeta+} \\ A_2 & \text{if } x \in \mathcal{M}_{\zeta-} \\ A_3 & \text{if } x \in \mathcal{L}_{\xi-} \end{cases}\,.$$

Finally,

$$\tilde{m}_\xi(x) = \begin{cases} \mu A_1 + (1-\mu)A_2 & \text{if } x \in \mathcal{L}_{\xi+} \\ A_3 & \text{if } x \in \mathcal{L}_{\xi-} \end{cases}\,,$$

with weak-$\lim_{\zeta\to\infty} \tilde{m}_{\xi,\zeta} = \tilde{m}_\xi$ in $L^2(\omega;\mathbb{R}^2)$ and weak-$\lim_{\xi\to\infty} \tilde{m}_\xi = m$ in $L^2(\omega;\mathbb{R}^2)$. Eventually, we got a sequence approaching weakly a constant function on O. We refer to [32] where it is shown that the sequence above is really minimizing. The minimizing sequence is obtained by the appropriate scaling of the picture on the right hand side of Figure 5. The strip of the thickness $1-\mu$ belongs to $\mathcal{L}_{\xi+}$, and the strip of thickness μ to $\mathcal{L}_{\xi-}$. Similarly, strips of the width μ and $1-\mu$ are subsets of $\mathcal{M}_{\zeta+}$ and $\mathcal{M}_{\zeta-}$, respectively.

Another representation of the relaxation of $\mathcal{E}_0$ is using the convex envelope φ^{**} of φ. We recall that the convex envelope is the supremum of all affine functions not greater than φ. We remark that φ^{**} can be explicitly calculated in particular cases. See [32] for some examples. The problem now reads: Minimize

$$\tilde{\mathcal{E}}_0 : \tilde{\mathcal{A}} \to \mathbb{R}\,, \quad \tilde{\mathcal{A}} = \Big\{\phi \in L^2(\omega,\mathbb{R}^n)\Big|\ |\,\phi\,| \le 1 \text{ a.e. in } \omega\Big\}\,, \tag{2.3}$$

where

$$\tilde{\mathcal{E}}_0(m) = \int_\omega \varphi^{**}(m)\,\mathrm{d}x + \frac{1}{2}\int_{\mathbb{R}^n} |\,\nabla u\,|^2\,\mathrm{d}x - \int_\omega \langle H, m\rangle_{\mathbb{R}^n}\,\mathrm{d}x\,, \quad \Delta u = \mathrm{div}\big(\chi_\omega m\big) \quad \text{in } \mathbb{R}^n\,. \tag{2.4}$$

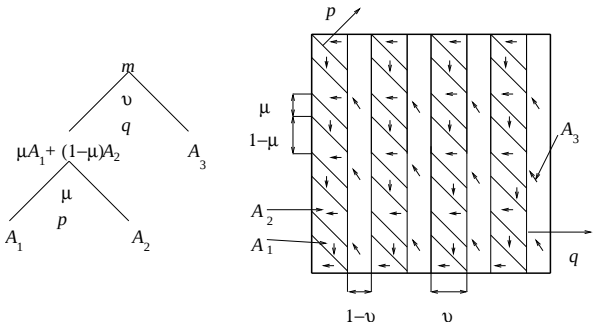

FIGURE 5. Construction of a minimizing sequence on O.

Minima of $\tilde{\mathcal{E}}_0$ may be characterized as solutions of corresponding Kuhn-Tucker equations: Find $(m, u, \lambda) \in L^2(\omega, \mathbb{R}^n) \times H^1(\mathbb{R}^n) \times L^2(\omega)$, such that

$$(\nabla u, \nabla w) = (m, \nabla w) \quad \forall\, w \in H^1(\mathbb{R}^n)\,, \tag{2.5}$$

$$\nabla u + D\varphi^{**}(m) + \lambda m = H \quad \text{a.e. in } \omega\,, \tag{2.6}$$

$$0 \le \lambda\,, \quad |\,m\,| \le 1\,, \quad \text{and} \quad \lambda(1 - |\,m\,|)_+ = 0 \quad \text{a.e. in } \omega\,. \tag{2.7}$$

Here, $(s)_+ := \max\{s, 0\}$ denotes the non-negative part, and the last condition in (2.7) states that $\lambda \neq 0$ is possible only for $|\,m\,| = 1$ as a consequence of $\lambda m \in \partial\mathfrak{Z}(m)$ for the convex characteristic functional $\mathfrak{Z} : \mathbb{R}^2 \to [0, \infty]$ defined by $\mathfrak{Z} = 0$, if $|\,m\,| \le 1$, and $\mathfrak{Z} = \infty$, if not.

The subsequent sections survey both, analytical and numerical aspects of these strategies to describe magnetization configurations on microscopic and mesoscopic levels. We begin with an interesting recent interpretation of Landau-Lifshitz model as a limiting problem of a statistical approach. Section 2.2 discusses scaling properties of domains and walls in terms of physical ($\alpha, \beta \ge 0$) and geometric ($\ell, \delta \ge 0$) parameters, and numerics in Subsection 2.2.1. Section 2.3 deals with Landau-Lifshitz energy without exchange energy; in particular, we evidence high complexity of algorithms in the course of direct minimization of $\mathcal{E}_0 : \mathcal{A}_h \to \mathbb{R}$ for finite-dimensional subsets $\mathcal{A}_h \subset \mathcal{A}$ in Section 2.3.1, which historically came first in numerical analysis of minimizing (1.4); in Section 2.3.2, strategies to discretize the degenerate elliptic problem (2.5)–(2.7) are reviewed; in Section 2.3.3, a convergent scheme using discretized Young measures to minimize the linear-quadratic problem is discussed. Section 2.4 discusses a reduced model in the thin film limit.

2.1. **Statistical theory derivation of the Landau-Lifshitz model.** The statistical mechanics of lattice spin system with a continuous order parameter is capable of describing equilibrium states of magnetic media. In relatively small scale devices thermal fluctuations affect the behavior of magnetic domain walls which need to be incorporated into the continuum model. Katsoulakis, Plecháč, and Tsagkarogiannis [55, 56] derived this limiting problem from statistical mechanics considerations using the large deviation theory. They consider an n-dimensional periodic lattice. At each side x of this lattice there is an order parameter σ representing the magnetic spin moment with values on the unit sphere S^{n-1}.

A most probable configuration of the system is then given by the Maxwellian distribution depending on (x, v), $v \in S^{n-1}$,

$$M(x, v) = \frac{1}{Z_b(x)} \exp\Big(-b\big(\varphi(v) + \langle v, \nabla\bar{u} - J * \bar{m} - H\rangle_{\mathbb{R}^n}\big)\Big)\,.$$

Here, J describes local mean field interaction in the exchange energy and Z_b is the corresponding partition function with $b = (kT)^{-1}$, for k Boltzmann's constant and T the absolute temperature. Moreover, $(\bar{u}, \bar{m})$ minimize a new free energy

$$E_b(m) = \frac{1}{2}\int_{\mathbb{R}^n} |\nabla u|^2\,\mathrm{d}x - \frac{1}{2}\int_\omega \langle J * m, m\rangle_{\mathbb{R}^n}\,\mathrm{d}x + \int_\omega a_b^*(m)\,\mathrm{d}x - \int_\omega \langle H, m\rangle_{\mathbb{R}^n}\,\mathrm{d}x\,, \tag{2.8}$$

where "*" stands for the convolution and a_b^* for the Legendre-Fenchel transform of

$$a_b(p) = \beta^{-1}\log\int_{S^{n-1}} \exp\big(-b(\varphi(v) + \langle v, p\rangle_{\mathbb{R}^n})\big)\,\mathrm{d}v\,.$$

Expanding the convolution term in (2.8) one gets the finite temperature analogy of the Landau-Lifshitz energy (1.4). An important point is that the energy (2.8) is minimized subject to the constraint $|m| \leq 1$, while the Landau-Lifshitz energy is considered for $|m| = 1$. The earlier mentioned convex constraint is due to thermal fluctuations, and the Landau-Lifshitz energy can be seen as the low temperature limit of the energy (2.8).

2.2. **The Landau-Lifshitz energy: a microscopic model.** The presence of the exchange energy contribution in the energy functional (1.4) is the reason for a variety of microscopic, multiscale magnetic phenomena like domains, structured domain walls, branching of domains, closure domains, etc. Construction of solutions $m = \operatorname{argmin}_{\mathcal{A}\cap H^1(\omega,\mathbb{R}^n)}\mathcal{E}_\alpha(\phi)$ is by minimizing sequences $\{m_\ell\}_\ell \subset \mathcal{A}\cap H^1(\omega,\mathbb{R}^n)$, which possess weakly convergent subsequences $\{m_\ell\}_\ell \in H^1(\omega,\mathbb{R}^n)$ where, by a compactness argument, its limit $m^* \in H^1(\omega,\mathbb{R}^n)$ also satisfies $|\,m^*\,| = 1$, for a.e. $x \in \omega$. Passing to the limit with respect to each energy contribution now follows by weakly lower (semi-)continuity property of each involved energy contribution. Explicit solutions

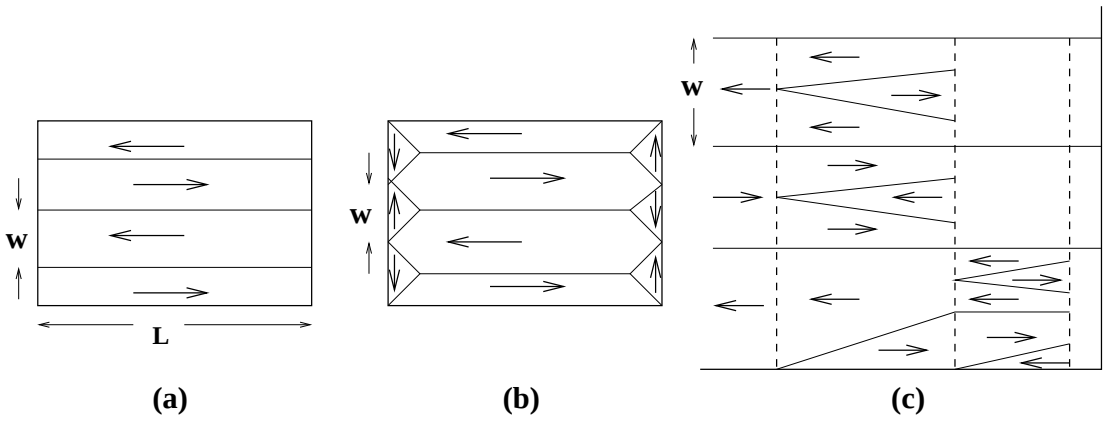

FIGURE 6. Multiscale phenomena and scaling laws in a uniaxial ferromagnet: (a) oscillatory magnetization pattern of layer width w, (b) closure domains added to eliminate surface charges, (c) domain branching due to Privorotskii [87] (sketch)

are only known in special cases [68, 85].

Example 2.1. *Let $\omega = \mathbb{R}^3$, $\xi_i \in \mathbb{R}^3$ be the unit vector in x_i-direction, and $e = \xi_3$. Suppose $m = m(x_1)$, and $\lim_{x_1\to\pm\infty} m(x_1) = \pm\xi_3$, then stray field contributions in the Landau-Lifshitz energy (without external field) can be computed, and hence*

$$\mathcal{E}_\alpha(m) = \int_{-\infty}^{+\infty} \alpha\,|\,m'\,|^2 - \langle m, Tm\rangle_{\mathbb{R}^3}\,\mathrm{d}x_1\,, \qquad T = \beta\,\xi_3\otimes\xi_3 - \xi_1\otimes\xi_1\,. \tag{2.9}$$

Parameterization of m using angles $(\,\vartheta,\iota\,) = (\,\frac{\pi}{2}-\phi, \frac{\pi}{2}-\theta\,) \in [0,\pi]\times[-\pi,\pi]$, cf. Figure 3 (a) yields to a representation

$$m(\vartheta,\iota) = \cos(\vartheta\xi_3) + \sin\big(\vartheta t(\iota)\big)\,, \qquad t(\iota) = \sin(\iota\xi_1) + \cos(\iota\xi_2)\,,$$

and the minimizer of (2.9) has the form

$$\vartheta(x_1) = \arccos\big(\tanh\frac{x_1}{w}\big)\,, \qquad \iota(x_1) = 0\,,$$

with $w = \sqrt{\frac{\alpha}{\beta}}$. Hence, the magnetization is nearly parallel to the easy axis at large distances from the origin, and these domains are separated by a Bloch domain wall $(\,-\delta,\delta\,)$ centered around the origin.

For highly anisotropic, uniaxial materials, domain branching and domains of specific scales are experimentally observed multiscale phenomena which may be explained as energy-minimizing mechanism in the context of micromagnetic theory. Figure 6 (a) shows oscillatory patterns of magnetizations of strongly uniaxial ferromagnets along the easy axis to avoid volume charges, whereas 'closure domains' are added in Figure 6 (b) along the boundary to also avoid surface charges at the expense of small anisotropy and surface

energy contributions. Finally, multiscale oscillatory structures are arranged in a complex branching pattern on surfaces perpendicular to the easy axis in the vicinity of $\partial\omega$ (see Figure 6 (c)).[1] In [24, 25], a simplified energy $\underline{\mathcal{E}} : \underline{\mathcal{A}} \to \mathbb{R}$, for $\underline{\mathcal{A}} = \{\phi \in BV(\omega, \mathbb{R}^n) \,|\, |\,\phi\,| = 1 \text{ a.e.}\}$, and $\omega = (0,\ell) \times \omega' \subset \mathbb{R}^n$ is considered,

$$\underline{\mathcal{E}}(m) = \alpha \,|\, Dm \,|(\omega) + \beta \int_\omega m_2^2 + m_3^2 \,\mathrm{d}x + \frac{1}{2} \int_{\mathbb{R}^3} |\, \nabla u \,|^2 \,\mathrm{d}x\,,$$

to study branching and inherent scalings for strongly uniaxial materials. Here, $|\, Du \,|(\cdot)$ denotes total variation of u. This 'wall' energy is chosen to restrict to sharp interfaces: it allows for jumps of m across a surface and assigns to them an energy which is proportional to the jump hight and surface area, neglecting possible internal wall structure (see below). In this case layers of width $w_{\min} \sim \sqrt{\alpha\ell}$ generate magnetization patterns of energy $\underline{\mathcal{E}}_{\min} \sim \sqrt{\alpha\ell}$ (Figure 6 (a)), which may be reduced to $\underline{\mathcal{E}}_{\min} \sim \sqrt{\alpha\beta\ell}$ for $w_{\min} \sim \sqrt{\frac{\alpha\ell}{\beta}}$ by using closure domains in Figure 6 (b) in case $\beta < 1$. Finally, Privorotskii's branching construction [87] to balance surface and anisotropy energies of closure domains creates significantly lower energies $\sqrt[3]{\alpha^2\ell \min\{\beta, 1\}}$ for typical bulk domain sizes $w_{\min} = \sqrt[3]{\frac{\alpha\ell^2}{\min\{\beta,1\}}}$, provided samples are sufficiently large to allow for branching structures, i.e., $\ell \gg \max\{\frac{\alpha}{\beta}, \alpha\}$, and $\sqrt[3]{\frac{\alpha\ell^2}{\min\{\beta,1\}}} \ll 1$. These scaling laws evidence sharpness of above branching constructions and hence detect domain branching as one essential multiscale phenomenon in micromagnetism. However, it is not clear from the energy-based arguments what are characteristic length-scales in the planes $x = 0, \ell$. Also, one might imagine from Figure 6 (a)–(c) that three-dimensional structures of uniaxial materials achieve a better scaling law — a possibility, which is ruled out in [25]. Finally, it is still not clear if corresponding observations hold for the exchange energy $\alpha \,\|\, \nabla m \,\|^2$ as well which moreover allows for internal wall structures of magnetizations.

Studies of inner structures of domain walls are one of the major research topics in nowadays micromagnetism. Existence, internal structure [6, 73], stability [37], and interaction [34] of different observed simple and complex domain walls exhibiting multiple scales (Figure 1) may also be understood for specific ranges of material and geometric parameters by Landau-Lifshitz energy (1.4). For thin soft ferromagnetic films $\omega = (0,\ell)^2 \times (0,\delta)$, $\delta > 0$ and practically relevant parameter regimes, $2d$ Néel walls are the favorite wall type, yielding to minimizing energies of magnitude $\mathcal{O}\big(\delta^2 \log^{-1}(\frac{\delta}{\alpha^2})\big)$; cf. Section 2.4, and [34, 33]. These theoretical studies of Néel walls support experimental observations in thin samples according to which they consist of a small core with fast varying rotation and two far-reaching, logarithmically decaying tails. Melcher [73] has given a more detailed analysis providing corresponding scaling laws of the pointwise behavior of the one-dimensional Néel wall, if confined by anisotropy energy. Understanding interaction of such walls with one another or with the boundary using Landau-Lifshitz energy is a subject of current research. Another recent result [37] establishes stability of one-dimensional Néel walls in thin films under two-dimensional perturbations; derived scaling laws for minimizing energies also evidence why energetically favorable cross-tie walls in moderately thick films are replaced by Néel-walls as thickness of the sample decreases. These results provide the basis to better understand structure and scalings of more complex walls, as e.g. cross-tie walls which are composed of Néel walls (cf. Figure 1 (c)); we refer to [34] for further discussion.

2.2.1. *Algorithms to minimize the Landau-Lifshitz energy.* If restricted to the first energy contribution in (1.4), stationary points to (1.4) are called harmonic maps, which are by now well-understood w.r.t. properties like existence, nonuniqueness, regularity and singularities of both, minimizing or nonminimizing harmonic maps. Numerically, it is challenging to meet energy decay property $\mathcal{E}_\alpha(m_h^j) \le \mathcal{E}_\alpha(m_h^{j-1})$, $j \ge 1$ with the nonconvex side-constraint $|\, m^j \,| = 1$ in an iterative context $j \ge 0$. Guided by analytical arguments above, there are efficient (non-conforming) numerical strategies [28, 31, 29, 69] to discretize the minimization problem by first minimizing the extension of $\mathcal{E}_\alpha$ to $H^1(\omega, \mathbb{R}^n)$, $\tilde{\mathcal{E}}_\alpha : H^1(\omega, \mathbb{R}^n) \to \mathbb{R}$ for $\beta = 0$, vanishing magnetic potential u, and zero external magnetic field and afterwards using stereographic projection (see Figure 7 (c)):

Algorithm 2.1. *1. Let $m^0 \in \mathcal{A}$ be an initial guess.*
2. For every $j \ge 1$, find $\tilde{m}^j \in H^1(\omega, \mathbb{R}^n)$ such that $\tilde{\mathcal{E}}_\alpha(\tilde{m}^j) \le \tilde{\mathcal{E}}_\alpha(m^{j-1})$.

[1] Note the closeness of the geometric construction in Figure 5 ($\alpha = 0$) to the one in Figure 6 (a),(b) ($\alpha > 0$).

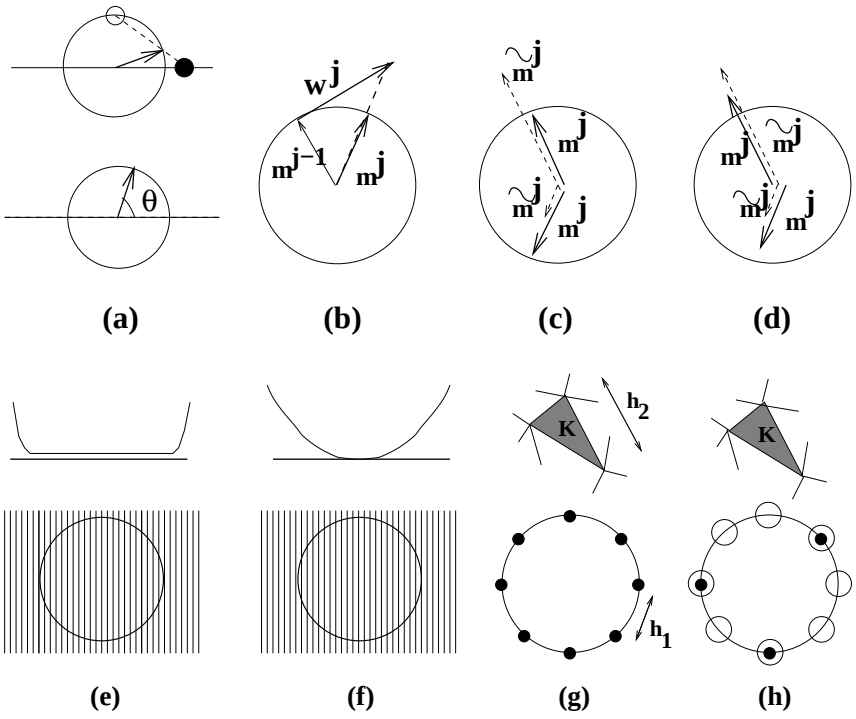

FIGURE 7. Discretization of nonconvex constraint: (a) local charts and parametrization, (b) convergent discretization by Alouges, (c) projection onto sphere, (d) scaled projection, (e) convexified problem, (f) including regularization, (g) discrete Young-measures, (h) including active-set strategy

3. Set $m^j = \frac{\tilde{m}^j}{|\tilde{m}^j|} \in \mathcal{A}$.
4. Set $j := j+1$ *and go to 2. until a stopping criterion is met.*

A conforming finite element realization of this algorithm confines the projection step to vertices of a quasiuniform mesh $\mathcal{T}_h$, and computes sequences $\{m_h^j\}_j \subset \mathcal{A}_h$ from piecewise affine, globally continuous $\{\tilde{m}_h^j\}_j \subset V_h(\omega;\mathbb{R}^n)$, where

$$m_h^j \in \mathcal{A}_h \equiv \left\{ \phi_h \in V_h(\omega;\mathbb{R}^n) \,\middle|\, |\,\phi_h(x_i)\,| = 1 \ \text{ for all vertices } x_i \right\}.$$

However, mainly because of the lack of convexity of the constraint, convergence of these algorithms cannot always be verified. In particular, decrease of energy of this strategy can be shown if iterates $v \in H^1(\omega,\mathbb{R}^n)$ lie outside the unit ball, i.e., $|\,v(x)\,| \geq 1$, which then implies $|\,\nabla\Big(\frac{v(x)}{|\,v(x)\,|}\Big)\,|^2 \leq |\,\nabla v(x)\,|^2$, for a.e. $x \in \omega$. In 1997, Alouges [2] came up with an energy-decreasing algorithm for minimizing harmonic maps, where every iteration step starts with a minimization on a new composed space, followed by a stereographic projection step: if compared to previous numerical strategies from above, this projection step now updates defects minimized on the manifold tangent to the constraint — rather than new iterates itself; cf. Figure 7 (b). Let again $\tilde{\mathcal{E}_\alpha}$ stand only for the exchange energy.

Algorithm 2.2. *1. Let* $m^0 \in \mathcal{A}$ *be an initial guess.*
2. For every $j \geq 1$, *compute a minimizer* $w^j \in K_{m^{j-1}}$ *of*

$$\tilde{\mathcal{E}_\alpha}(m^{j-1}-w) \qquad \forall\, w \in K_{m^{j-1}} \equiv \left\{ w \in H_0^1(\omega,\mathbb{R}^n) \,\middle|\, \langle w, m^{j-1}\rangle_{\mathbb{R}^3} = 0 \ \ a.e.\ in\ \omega \right\}.$$

3. Set $m^j = \frac{m^{j-1}-w^j}{|m^{j-1}-w^j|}$.
4. Set $j := j+1$, *and go to 2. until a stopping criterion is met.*

A stopping criterion can be that the difference of two subsequent values of $\tilde{\mathcal{E}}_\alpha$, $\tilde{\mathcal{E}}_\alpha(m^{j-1}) - \tilde{\mathcal{E}}_\alpha(m^j)$ is sufficiently small. By construction of the numerical scheme, we have

$$|\, m^{j-1} - w \,|^2 = 1 + |\, w \,|^2 \geq 1 \quad \text{a.e. in } \omega\,,$$

which implies the energy estimate $\tilde{\mathcal{E}}_\alpha(m^j) \leq \tilde{\mathcal{E}}_\alpha(m^{j-1} - w^{j-1}) \leq \tilde{\mathcal{E}}_\alpha(m^{j-1})$ during the projection step; from a practical viewpoint, the lack of convexity has been transformed into the linear, easier to handle constraint $\langle m^j, w\rangle_{\mathbb{R}^3} = 0$, almost everywhere in ω. The following result is due to Alouges [2].

Theorem 2.1. *Algorithm 2.2 converges in the sense that a (relabeled) subsequence $\{m^j\}_j$ weakly converges in $H^1(\omega,\mathbb{R}^3)$ to a harmonic map $m^\infty \in \mathcal{A} \cap H^1_{n_0}(\omega,\mathbb{R}^3)$, where n_0 is the boundary data of m^0. Moreover, the entire sequence $\{w^j\}$ strongly converges to zero in $H^1_0(\omega,\mathbb{R}^3)$.*

In [8], stability and convergence of a finite element realization of Alouges' algorithm for restricted triangulations with angles not exceeding $\pi/2$ is verified, and explicit counterexamples are presented (2D, 3D), which show increase of energy for non-permitted triangulations. — These results apply to harmonic maps, whereas Landau-Lifshitz energy also accounts for nonlocal effects in terms of stray field energy; recently in [3], Alouges' scheme is extended to the micromagnetic energy $\mathcal{E}_\alpha$, by accounting for nonlocal stray field energies, in particular. The splitting-type algorithm extends the layout of Algorithm 2.2 by introducing an additional parameter $\lambda > 0$.

Algorithm 2.3. *1. Let $m^0 \in \mathcal{A}$ be an initial guess.*
2. For every $j \geq 1$, compute a minimizer $w^j \in K_{m^{j-1}}$ of

$$\alpha \int_\omega |\, \nabla(m^{j-1} - w) \,|^2 \,\mathrm{d}x + \int_\omega \varphi(m^{j-1} - w)\,\mathrm{d}x + \frac{1}{2}\int_\omega \langle \nabla\Delta^{-1}\mathrm{div}\, m^{j-1}, m^{j-1} - w\rangle_{\mathbb{R}^n}\,\mathrm{d}x - \int_\omega \langle H, m^{j-1} - w\rangle_{\mathbb{R}^n}\,\mathrm{d}x\,.$$

3. Set $m^j = \frac{m^{j-1} - \lambda w^j}{|\, m^{j-1} - \lambda w^j \,|}$.
Set $j := j + 1$ and go to 2. unless a stopping criterion is met.

Different scaling properties of exchange energy and stray field energy contributions in terms of $\lambda > 0$ yield to energy decay of the method during projection and hence convergence for sufficiently small choices $\lambda < \lambda_0$.

Remark 2.1. *Possible strategies to conserve $|\, m \,| = 1$ may be based on parameterization of S^{n-1} or local charts for the sphere, cf. Figure 7 (a), which often leads to efficient numerical methods in the two-dimensional case. However, these ansatzes restrict possible minimizers to* (1.4) *and dynamics (see Section* (3)*), or require strategies to change between charts of the sphere.*

2.3. **The relaxed Landau-Lifshitz energy without exchange energy: a mesoscopic model.** Microscopic magnetization patterns described as minima of (1.4) reveal multiple scales, with smallest oscillations exhibiting a scale $\alpha > 0$, allowing for infinitely many oscillations for minimizers $m \in L^\infty(\omega,\mathbb{R}^n)$ in the limiting case $\alpha \to 0$. Section 2.3.1 considers mesh-dependent discrete minimizers of $\mathcal{E}_0 : \mathcal{A}_h \to \mathbb{R}$ of multiple scales to illustrate possible smearing of physical patterns (for $\alpha > 0$) due to discretization effects; this section bridges over to the study of the degenerate elliptic problem (2.5)–(2.7). Existing results on the relaxation (2.2) using Young measures are reviewed in Section 2.3.3.

2.3.1. *Discretization of the nonconvex problem.* We highlight numerical effects imposed to $m_h = \mathrm{argmin}_\phi \mathcal{E}_0(\phi) \in \mathcal{A}_h$ by the underlying mesh $\mathcal{T}_h$ and their scalings to allow for reliable resolution of relevant structures of $m = \mathrm{argmin}_\phi \mathcal{E}_\alpha(\phi) \in \mathcal{A} \cap H^1(\omega,\mathbb{R}^n)$, $\alpha > 0$ small. In [88], magnetization patterns are constructed for minimizers $m_h = \mathrm{argmin}_\phi \tilde{\mathcal{E}}_0(\phi) \in \tilde{\mathcal{A}}_h \equiv \left\{\phi_h\big|_K \in [\mathcal{P}_0(K)]^n\,,\ \forall\, K \in \mathcal{T}_h\right\}$ for uniaxial materials in the absence of exterior forces, i.e.,

$$\tilde{\mathcal{E}}_0(\phi_h) = \beta \int_\omega |\, \langle \phi_h, e_\perp\rangle_{\mathbb{R}^n} \,|^2\,\mathrm{d}x + \frac{1}{2}\int_{\mathbb{R}^n} |\, \nabla\Delta^{-1}\mathrm{div}(\chi_\omega\, \phi_h) \,|^2\,\mathrm{d}x\,. \tag{2.10}$$

Above and in the sequel $\mathcal{P}_d(K)$, $d = 0, 1$ denotes spaces of polynomials of degree $\leq d$ on K. Minimizing constructions motivate a geometry which bridges laminate structures of scale $\mathcal{O}(h^{1/3})$ in the bulk of the specimen to closure domain structures of scale $\mathcal{O}(h^{2/3})$ at the boundary $\partial\omega$ over a length-scale $\mathcal{O}(1)$ in order to optimally balance interpolation errors on a quasiuniform mesh, cf. Figure 8. Computing energy

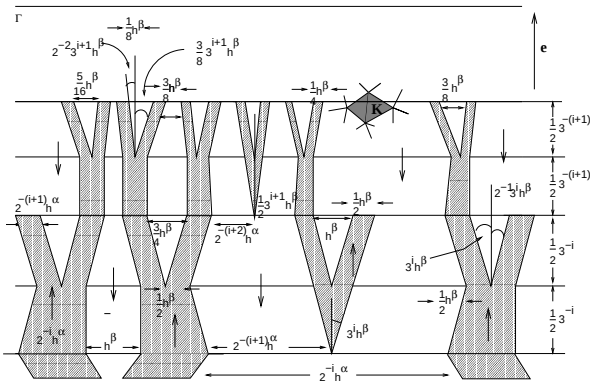

FIGURE 8. Construction of branching magnetization m_h, using direct minimization (uniaxial; from [88])

contributions in (2.10) which arise from interpolating this structure onto the mesh gives the upper bound for uniaxial materials [88],

$$\min_{\phi_h \in \tilde{\mathcal{A}}_h} \tilde{\mathcal{E}}_0(\phi_h) \leq C\big(1 + \log_3 \frac{1}{h}\big) h^{2/3} .$$

Interestingly, scales differ for discrete minimizing magnetizations of cubic ferromagnets, where laminates in the interior of the ferromagnet of magnitude $\mathcal{O}(1)$ are reduced to closure domains $\mathcal{O}(h)$ by multiple branching over a length-scale of $\mathcal{O}(1)$, cf. [88].

2.3.2. *Discretization of the convexified problem.* Computation of mesoscopic magnetization is more efficient if (2.5)–(2.7) is used rather than dealing with the minimization problem $\tilde{\mathcal{E}}_0 : \tilde{\mathcal{A}} \to \mathbb{R}$ directly, in cases where the convex envelope $\varphi^{**} : \mathbb{R}^n \to \mathbb{R} \cup \{+\infty\}$ is explicitly known. These equations are degenerate elliptic, so solutions $(m, u, \lambda) \in L^2(\omega, \mathbb{R}^n) \times H^1(\mathbb{R}^n) \times L^2(\omega)$ are not unique in general. However, they are unique for uniaxial materials in two or three dimensions (cf. [18] for two dimensions). We recall a proof in two dimensions, see [62] for $n = 3$. Note that the difference of two possible solutions $(\delta, e) := (m_2 - m_1, u_2 - u_1)$ to (2.5)–(2.7) is determined by

$$\| \nabla e \|^2_{L^2(\mathbb{R}^2)} + \int_\omega \big\langle D\varphi^{**}(m_2) - D\varphi^{**}(m_1), \delta \big\rangle_{\mathbb{R}^2} \, \mathrm{d}x + \int_\omega \big\langle \lambda_2 m_2 - \lambda_1 m_1, \delta \big\rangle_{\mathbb{R}^2} \, \mathrm{d}x = 0 . \tag{2.11}$$

By monotonicity arguments, it is easy to see that all terms are non-negative and hence vanish, yielding to

$$e = 0 , \qquad \operatorname{div} \delta = 0 \quad \text{a.e. in } \omega, \qquad \langle \delta, n \rangle_{\mathbb{R}^2} = 0 \quad \text{a.e. on } \partial\omega,$$

where for a moment n denotes the outer unit normal to $\partial\omega$. Here, the last two results are outcomes from the first one, using (1.1). Consider the divergence-free function $\tilde{\delta} \in L^2(\mathbb{R}^2, \mathbb{R}^2)$, with $\tilde{\delta}\big|_\omega = \delta$, and $\tilde{\delta} = 0$ else; there holds $\tilde{\delta} \in H(\mathrm{div}; \mathbb{R}^2)$, since normal components of $\tilde{\delta}$ are continuous on the boundary $\partial\omega$. By Helmholtz decomposition principle, $\tilde{\delta} = \operatorname{curl} \eta$, $\eta \in W^1(\mathbb{R}^2)$, with $\eta = \text{const}$, since $\tilde{\delta} = 0$ outside $\omega \subset \mathbb{R}^2$. But $\nabla\eta \parallel e$, thanks to (2.11), and $\eta = 0$ outside $\overline{\omega}$, which eventually proves $(e, \delta) = (0, 0)$. These arguments do not carry over to cubic materials.

A canonical conforming finite element discretization of (2.5)–(2.7) asks for solutions $(m_h, u_h) \in W_h(\omega; \mathbb{R}^n) \times V_h(\mathbb{R}^n)$, where $V_h(\cdot)$ is assembled from elementwise affine, globally continuous functions, and $W_h(\cdot)$ gathers elementwise constant grid functions on a quasi-uniform mesh $\mathcal{T}_h$ of $\mathbb{R}^n$, such that $\mathcal{T}_h\big|_\omega$ is a triangulation of $\omega \subset \mathbb{R}^n$; the non-stable behavior is illustrated by the computations in Figure 9 (a). Mathematically, this observation may be explained by the lack of validity of discrete Helmholtz principle for the used finite element pairing, which was the crucial tool to verify uniqueness of solutions for the limiting problem (2.5)–(2.7) in the above argument. This short-coming of a discretization is cured if $V_h(\cdot)$ is replaced by Crouzeix-Raviart based elements

$$\tilde{V}_h(\Omega) = \Big\{ \phi_h \in L^2(\Omega) \big| \ \phi_h\big|_K \in \mathcal{P}_1(K), \ \int_{\overline{K} \cap \overline{K'}} \phi_h \, \mathrm{d}s = 0 \quad \forall K, K' \in \mathcal{T}_h \Big\} ,$$

for polyhedral $\Omega \subseteq \mathbb{R}^n$, which now allows for discrete Helmholtz principle of involved spaces, leading to a well-posed discretization [18] of (2.5)–(2.7) (uniaxial materials). In [18], a penalized version of this problem is then studied, and nonlocal magnetostatic effects are accounted for on a set $\mathbb{R}^n \supseteq \Omega \supset \omega$, using vanishing Dirichlet data for magnetic potential, i.e., $u_h \in \tilde{V}_h^0(\Omega)$; see also Figure 7 (e).

Problem 2.1. *Find* $(m_h, u_h) \in W_h(\omega;\mathbb{R}^n) \times \tilde{V}_h^0(\Omega)$ *such that*

$$
\begin{aligned}
&(\nabla_h u_h, \nabla_h w_h) = (m_h, \nabla_h w_h) \quad \forall\, w_h \in \tilde{V}_h^0(\Omega)\,,\\
&\nabla_h u_h + D\varphi^{**}(m_h) + \lambda_h m_h = P_h H \qquad \lambda_h = \varepsilon^{-1}\frac{(|\,m_h\,|-1)_+}{|\,m_h\,|} \qquad \textit{a.e. in } \omega\,.
\end{aligned}
$$

A proof of the following error statement for solutions to Problem 2.1 (uniaxial case) exploits discrete Helmholtz principle for the used finite pairing and a bootstrapping argument [18],

$$
\|\,\nabla(u-u_h)\,\|^2_{L^2(\Omega)} + \|\,D\varphi^{**}(m) - D\varphi^{**}(m_h)\,\|^2_{L^2(\omega,\mathbb{R}^2)} + \|\,\lambda m - \lambda_h m_h\,\|^2_{L^2(\omega,\mathbb{R}^2)} \leq C\big(\varepsilon + h\big)\,. \tag{2.12}
$$

An alternative strategy to obtain a stable discretization of (2.5)–(2.7) is to go back to the formerly mentioned

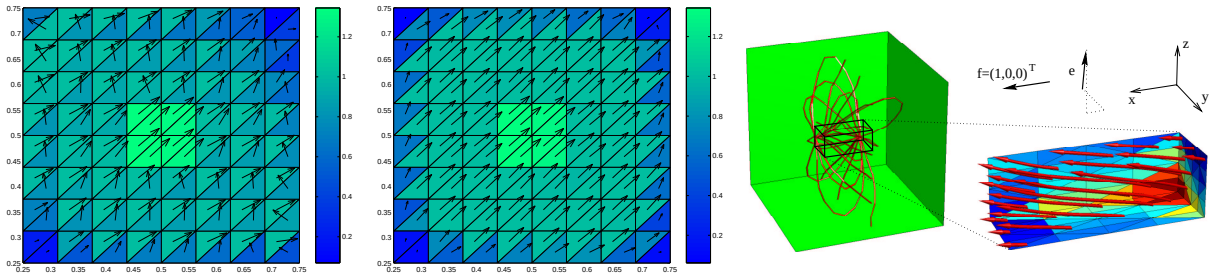

FIGURE 9. Convexification: magnetization of (a) unstable scheme, (b) stable scheme (Problem 2.1), (c) stabilized scheme (Problem 2.2, $\ell = A$) (from [88])

scenario $(m_h, u_h) \in W_h(\omega;\mathbb{R}^n) \times V_h^0(\Omega)$, and adding stabilizing terms which control non-physical oscillatory behavior.

Problem 2.2. *Find* $(m_h, u_h) \in W_h(\omega;\mathbb{R}^n) \times V_h^0(\Omega)$ *such that for* $\ell \in \{A, B\}$

$$
\begin{aligned}
&(\nabla u_h, \nabla w_h) = (m_h, \nabla w_h) \quad \forall\, w_h \in \tilde{V}_h^0(\Omega)\,,\\
&(\nabla u_h, \mu_h) + (D\varphi^{**}(m_h), \mu_h) + (\lambda_h m_h, \mu_h) + t_\ell([m_h],[\mu_h]) = (H, \mu_h) \quad \forall\, \mu_h \in W_h(\omega,\mathbb{R}^n)\,,\\
&\lambda_h = \varepsilon^{-1}\frac{(|\,m_h\,|-1)_+}{|\,m_h\,|} \qquad \textit{a.e. in } \omega\,.
\end{aligned}
$$

Here, $[\cdot] : L^\infty(K \cup K', \mathbb{R}^n) \to L^2(\overline{K} \cap \overline{K'}, \mathbb{R}^n)$, for adjacent $K, K' \in \mathcal{T}_h\big|_\omega$ denotes the jump across inter-element interior faces $\xi \equiv \overline{K} \cap \overline{K'} \in \Xi$. The following stabilizations are considered in [88], for $n = 2$,

$$
t_A([m_h],[\mu_h]) = \sum_{\xi\in\Xi} h_\xi \int_\xi [\langle m_h, n\rangle_{\mathbb{R}^2}][\langle \mu_h, n\rangle_{\mathbb{R}^2}]\,\mathrm{d}x\,, \qquad t_B([m_h],[\mu_h]) = \sum_{\xi\in\Xi} h_\xi \int_\xi \langle [m_h],[\mu_h]\rangle_{\mathbb{R}^2}\,\mathrm{d}x\,.
$$

Problem 2.2 produces solutions which enjoy (2.12) for slightly restricted mesh-geometries; its convergence proof avoids the above argument based on discrete Helmholtz-principle and uses inverse-type inequalities instead. Behavior of this stabilized method can be motivated by interpreting Problem 2.2 as Kuhn-Tucker equation of a slight modification of the strictly convex energy ($\varepsilon > 0$)

$$
\tilde{\mathcal{E}}_0(m) + \varepsilon \int_\omega \mathfrak{Z}_\ell(m)\,\mathrm{d}x\,, \qquad \mathfrak{Z}_A(m) = |\,\mathrm{div}\, m\,|^2 \quad \text{or} \quad \mathfrak{Z}_B(m) = |\,\nabla m\,|^2\,.
$$

Convergence result (2.12) allows for control of certain components of iterates $\{m_h\}_h$ as $h \to 0$, obtained from Problems 2.1 and 2.2; in general, strong convergence of $\{m_h\}_h$ may not be expected, due to the degenerate

convexity of the energy functional (2.4), which prevents us to reliably recover the uniquely defined Young measure in the uniaxial case (cf. [32] and Section 2.3.3)

$$x \mapsto \nu_x = \Gamma\big(m(x)\big)\delta_{m^+\left(m(x)\right)} + \Big(1-\Gamma\big(m(x)\big)\Big)\delta_{m^-\left(m(x)\right)}\,, \quad \text{where} \tag{2.13}$$

$$m^{\pm}\big(m(x)\big) = \pm\Big(1-\langle m(x),e_\perp\rangle^2_{\mathbb{R}^2}\Big)^{1/2} e + \langle m(x),e_\perp\rangle_{\mathbb{R}^2} e_\perp\,, \quad \Gamma\big(m(x)\big) = \tfrac{1}{2} + \frac{\langle m(x),e\rangle_{\mathbb{R}^n}}{2\left(1-\langle m(x),e_\perp\rangle^2_{\mathbb{R}^2}\right)^{1/2}}$$

in a post-processing step. Surprisingly, numerical schemes can be constructed for the uniaxial case which compute magnetizations that strongly converge to solutions of (2.5)–(2.7), and which are motivated from

$$\tilde{\mathcal{E}}_0(m) + \varepsilon_1 \int_\omega |\,\nabla m\,|^2\,\mathrm{d}x + \varepsilon_2 \int_\omega |\,\nabla^2 m\,|^2\,\mathrm{d}x\,, \qquad \varepsilon_i > 0\,. \tag{2.14}$$

The following scheme uses piecewise affine finite elements for the magnetization field as well [88]; cf. Figure 7 (f).

Problem 2.3. *Find* $(m_h, u_h) \in V_h(\omega,\mathbb{R}^2) \times V_h^0(\Omega)$ *such that*

$$\begin{aligned}
&(\nabla u_h, \nabla w_h) = (m_h, \nabla w_h) \quad \forall\, w_h \in V_h^0(\Omega)\,,\\
&(\nabla u_h, \mu_h) + (\langle m_h, e_\perp\rangle_{\mathbb{R}^2}, \langle \mu_h, e_\perp\rangle_{\mathbb{R}^2}) + (\lambda_h m_h, \mu_h)\\
&\qquad + h\sum_{\xi\in\Xi}\int_\xi \big\langle [\partial_n m_h], [\partial_n \mu_h]\big\rangle_{\mathbb{R}^4} + h^{3/2}(\nabla m_h, \nabla \mu_h) = (H, \mu_h)\,, \quad \forall\, \mu_h \in V_h(\omega,\mathbb{R}^2)\,,\\
&\lambda_h = h^{-2}\frac{(|\,m_h\,|-1)_+}{|\,m_h\,|} \qquad \textit{a.e. in } \omega\,.
\end{aligned}$$

Note the scaling for λ_h, which is different from the one in Problems 2.1 and 2.2. Next to (2.12), the following results apply [88],

$$\frac{\sqrt{h}}{2}\Big(\sum_{\xi\in\Xi}\int_\xi |\,[m-m_h]\,|^2\,\mathrm{d}x\Big)^{1/2} + h^{1/2}\|\,m-m_h\,\|_{L^2(\omega,\mathbb{R}^2)} + h^{3/4}\|\,\nabla(m-m_h)\,\|_{L^2(\omega,\mathbb{R}^4)} \le C\,h\,, \tag{2.15}$$

$$\|\,m-m_h\,\|_{L^2(\omega',\mathbb{R}^2)} \le C\Big(h^{5/8} + \mathrm{dist}^{-1/2}(\partial\omega,\omega')h^{3/4}\Big)\,, \tag{2.16}$$

provided that the solution to (2.5)–(2.7) is sufficiently regular; the proof is based on a Helmholtz-decomposition for $L^2(\omega,\mathbb{R}^2)$-functions, makes use of increased stability properties of the scheme, together with estimates for $\|\,m-m_h\,\|_{H^{-1}(\omega,\mathbb{R}^2)}$; finally, balancing the error in the interior of $\omega \subset \mathbb{R}^2$ and in a boundary layer close to $\partial\omega$ yields (2.15)–(2.16). Control of the related Young measure is now an immediate consequence.

Remark 2.2. *Computation of the nonlocal magnetostatic field* $-\nabla u$ *requires to solve* (2.5) *in the whole* $\mathbb{R}^n$. *There are different approaches to evaluating this field: first, truncation by restricting the magnetostatic field to the compact domain* Ω, *for* $\mathbb{R}^n \supset \Omega \ni \omega$ *and imposing Dirichlet data on* $\partial\Omega$, *see e.g.* [18, 88]. *Choosing* $\mathrm{diam}\,\Omega \approx 10\,\mathrm{diam}\,\omega$ *is motivated in* [40] *for practical studies in order to capture relevant magnetostatic energy contributions. Second,* (2.5) *is solved exactly in* [72, 71, 64, 86, 17] *via integral representation, i.e.,* $-\nabla u = -\nabla\mathcal{L}m$, *for a linear convolution operator* $\mathcal{L} : L^2(\mathbb{R}^n,\mathbb{R}) \to H^1(\Omega)$; *interesting numerical approaches using* $\mathcal{H}$*-matrix techniques in this context are proposed and studied in* [86]. — *We refer to Figure 10 for a comparison of these strategies to compute the stray field.*

2.3.3. *Discretization of the relaxed problem.* If the convex envelope φ^{**} is not known explicitly, minimizing $\overline{\mathcal{E}}_0$ from (2.2) yields to a measure valued solution which not only contains information about the mesoscopic magnetization m but also about a pattern of minimizing sequences. As to a numerical discretization of (2.2) we also must, besides a discretization of ω, discretize the sphere S^{n-1}; cf. Figure 7 (g). Let $\mathcal{T}^1_{h_1}$ be a quasiuniform triangulation of ω that consists of elements with diameter not exceeding h_1. Similarly, we define a triangulation $\mathcal{T}^2_{h_2}$ of S^{n-1} which is assembled from elements with a spherical diameter not exceeding h_2. Hence, we obtain a triangulation $\mathcal{T}_h = \mathcal{T}^1_{h_1} \times \mathcal{T}^2_{h_2}$ of $\omega \times S^{n-1}$ with mesh parameter $h = (h_1, h_2)$. We may now define projectors $P^1_{h_1} : L^1\big(\omega; C(\mathcal{S}^{n-1})\big) \to L^1\big(\omega; C(\mathcal{S}^{n-1})\big)$ by

$$[P^1_{h_1} G](x,A) = \frac{1}{|K|}\int_K G(y,A)\,\mathrm{d}y \qquad \forall\, x \in K \in \mathcal{T}^1_{h_1}\,,$$

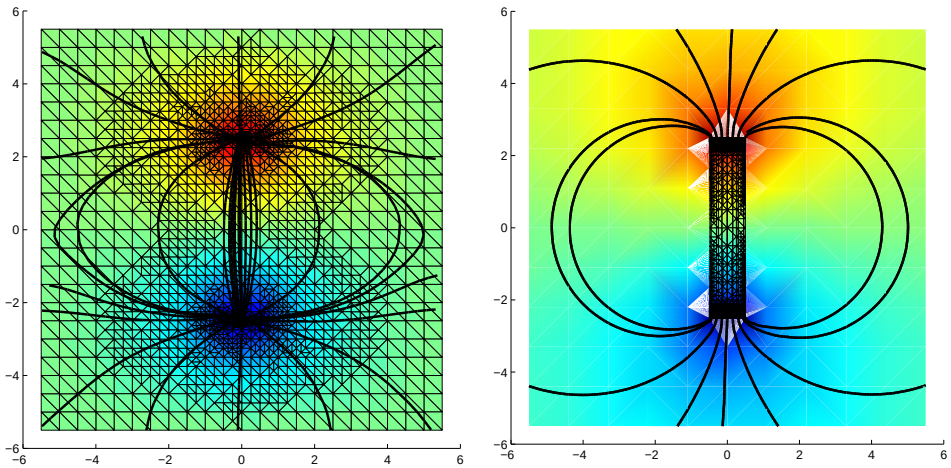

FIGURE 10. Stray field $-\nabla u_h$ around ferromagnet $\omega = (-0.5, 0.5) \times (-2.5, 2.5)$ displayed by level lines using truncated domain $\Omega = (-5.5, 5.5)^2$ (left), or FEM-BEM coupling (right) (from [16])

and $P^2_{h_2}(x,\cdot)$ denotes a projector that assigns to each $G(x,\cdot)$ its $\mathcal{T}^2_{h_2}$-elementwise affine, globally continuous interpolation, i.e., $[P^2_{h_2}G](x,A) = \sum_{i=1}^{L_{h_2}} G(x,A_i)v_i(A)$, for basis functions $\{v_i\}_i$ satisfying $v_i(A_j) = \delta_{ij}$; functions φ_i are nonnegative and $\sum_{i=1}^{L_{h_2}} v_i(A) = 1$. Then, the composed projector $P_h = P_{(h_1,h_2)} = P^1_{h_1}P^2_{h_2} = P^2_{h_2}P^1_{h_1}$ provides an ω-elementwise constant and $\mathcal{S}^{n-1}$-elementwise affine, globally continuous approximation, with adjoint projector $P^*_h : \overline{\mathcal{A}} \to \overline{\mathcal{A}}$ defined by $\langle \nu, P_h G\rangle = \langle P^*_h \nu, G\rangle$. The following characterization of $\overline{\mathcal{A}}_h = P^*_h\overline{\mathcal{A}} \subset \overline{\mathcal{A}}$ is taken from [89, Sec. 3.5],

$$\overline{\mathcal{A}}_h := \left\{ \nu^h = \{\nu^h_K\}_{K\in\mathcal{T}^1_{h_1}},\ \nu^h_K = \sum_{i=1}^{L_{h_2}} \lambda_{K,i}\delta_{A_i} \quad \forall\, K \in \mathcal{T}^1_{h_1} \right\},$$

where $\lambda_i\big|_K \equiv \lambda_{K,i}$ is $\mathcal{T}^1_{h_1}$-elementwise constant, such that $\sum_{i\geq 1}\lambda_i = 1$. A proper discretization of (2.2) can now be stated in the following form [64]; see Figure 7 (g).

Problem 2.4. *Find a minimizer* $(\mu^h, m^h, u^h) \in \overline{\mathcal{A}}_h \times W_{h_1}(\omega;\mathbb{R}^2) \times \tilde{V}^0_{h_1}(\Omega)$ *of* $\overline{\mathcal{E}}_0$ *subject to*

$$m_h\big|_{K\in\mathcal{T}^1_{h_1}} = \int_{S^{n-1}} A\mu^h_K(\mathrm{d}A), \qquad (\nabla_{h_1}u_{h_1}, \nabla_{h_1}w_{h_1}) = (m_{h_1}, \nabla_{h_1}w_{h_1}) \quad \forall\, w_{h_1} \in \tilde{V}^0_{h_1}(\Omega).$$

Problem 2.4 is convex, of quadratic-linear type and with linear constraint; a numerical analysis is given in [64], which verifies convergence of the method for a relative scaling $h_2 = o(h_1^{n/2})$. In practice, the size of this problem may be very large for sufficiently small h. In [64], and motivated from [19], an active-set strategy is proposed and analyzed which selects active atoms per each element $K \in \mathcal{T}_{h_1}$ independently according to a local convex optimization problem; see Figure 7 (h). This procedure drastically decreases complexity of the problem; we refer to [64] for details.

Remark 2.3. *Let us mention another possibility to approximate the relaxed problem by means of Young measures. Using the Caratheódory theorem we know that for any* $m(x) \in \mathbb{R}^n$, $|m(x)| \leq 1$ *there are at most* $n+1$ *points* A_i *on* S^{n-1} *such that* $\varphi^{**}(m) = \sum_{i=1}^{n+1}\lambda_i\delta_{A_i}$, *where functions* λ_i, $i = 1,\dots,n+1$ *are coefficients of a convex combination. Therefore, we can consider a Young measure* $\nu^h_K = \sum_{i=1}^{n+1}\lambda_{K,i}\delta_{A_i}$, *where* $K \in \mathcal{T}^1_{h_1}$, *and* $\{\lambda_{K,i}\}_i$ *are constant on* K. *Points* $\{A_i\}_i \in S^{n-1}$ *may again be described by means of angles in spherical coordinates to avoid the nonconvex constraint, and for each* $K \in \mathcal{T}^1_{h_1}$ *hold* $\{\lambda_{K,i}\} \geq 0$ *and* $\sum_{i=1}^{n+1}\lambda_{K,i} = 1$. *However, the resulting optimization problem is again highly nonconvex; see* [61] *for details.*

2.4. **Thin film limit.** Driven by needs of spin electronics ferromagnetic films enjoy renewed attention. Magnetization pattern are different from those in bulk materials because the magnetostatic interaction behaves differently if the magnetization $m : \omega \to \mathbb{R}^3$ remains uniform across the thickness of the film. Let $\omega = \omega' \times (0, \delta)$ be a cylindrical domain of radius ℓ and thickness $\delta > 0$, $\delta \ll \ell$, and $\varphi(m) = \beta\,(m_2^2 + m_3^2)$ for $m = (m_1, m_2, m_3)$, i.e., the easy axis is in the plane of the film. Under the assumptions that (i) the sample is not too small in the sense of $\alpha \ll \ell\delta \log^{-1}(\frac{\ell}{\delta})$, and (ii) anisotropy and external field are sufficiently weak in the sense of $\beta = \mathcal{O}(\frac{\delta}{\ell})$ and $|\,H\,| = \mathcal{O}(\frac{\delta}{\ell})$, it is shown in [34] that the limiting behavior of minimizers of (1.4) for $\delta \to 0$ may be represented by using the following Γ-convergent, two-dimensional reduced problem: Minimize

$$\tilde{\mathcal{E}}_{\rm thin}(m') = \frac{\beta}{\delta}\int_{\omega'} |\,m_2'\,|^2\,\mathrm{d}x' + \frac{1}{2}\int_{\Omega} |\,\nabla\tilde{u}\,|^2\,\mathrm{d}x - \frac{1}{\delta}\int_{\omega'} \langle H, m'\rangle_{\mathbb{R}^n}\,\mathrm{d}x' \tag{2.17}$$

amongst all $m' : \omega' \to \mathbb{R}^2$, $\tilde{u} : \Omega \to \mathbb{R}$, for $\Omega \subseteq \mathbb{R}^3$ containing ω, such that

$$|\,m'\,|^2 \le 1 \quad \text{in } \omega', \qquad (\nabla\tilde{u}, \nabla w)_\Omega = (m', \nabla' w') \quad \forall\, w \in H_0^1(\Omega)\,.$$

This result can be motivated by a simple scaling argument, according to which surface, anisotropy, and Zeeman's energy respectively are of magnitudes $\mathcal{O}(\alpha\delta)$, $\mathcal{O}(\beta\ell^2\delta)$, and $\mathcal{O}(|\,H\,|\ell^2\delta)$. The magnetostatic energy being nonlocal is more complicated but can be approximated by [40, 34]

$$\int_\Omega |\,\nabla u\,|^2\,\mathrm{d}x \approx \delta^2\int_\Omega |\,\nabla\tilde{u}\,|^2\,\mathrm{d}x + \delta\int_{\omega'} |\,m_3\,|^2\,\mathrm{d}x' = \mathcal{O}(\ell\delta^2) + \mathcal{O}(\ell^2\delta)\,.$$

This formula splits magnetostatic contributions into those which penalize in-plane divergence and out-of plane component separately.

In the regime $\delta \ll \ell$, the larger of the two magnetostatic terms is the cost of the out-of plane component m_3, which is why we expect $m_3 \approx 0$. Assuming now $m(x) = m(x')$, for $x' \in \mathbb{R}^2$, and using the above scalings for $\beta, |\,H\,|$, all terms — apart from the smaller surface exchange energy —, lead to contributions $\mathcal{O}(\ell\delta^2)$, which motivates (2.17). We refer to [36] for further details.

3. Dynamical models — from spin dynamics to mesoscopic evolution

Field-induced magnetization dynamics in a ferromagnetic field leads to domain wall motion to reach states of lower energy. During its motion, it may be trapped in local energy minima until thermal fluctuations allow to overcome one of the energy barriers that separate the system from neighboring favorable states; a full description of magnetization reversal needs to contain precisely the spatial and time dependence of the nucleation and domain wall structure at different fields: at low fields, and for an initially saturated sample, nucleation always initiates at low anisotropic extrinsic defects or at film edges; in contrast, at high fields, intrinsic nucleation takes place in many low coercivity regions, e.g., correlated with film polycrystallinity in composed matter. Rough domain walls move in a jerky manner by successive micrometer-sized jumps at the wall boundary; moreover, submicron-sized defects and film nanostructure are further impediences of domain wall propagation at lower scales.

The most rigorous micromagnetic model is the Landau-Lifshitz model. However, this microscopic description models phenomena reasonable only for small areas of submicron size, and cannot model large Barkhausen jumps, for example. Moreover, relevant time-scales are of picoseconds, and the relaxation of magnetization can be examined only across no more than some nanoseconds. These shortcomings are amongst the main motivations for mesoscopic models to describe magnetization reversal.

3.1. **The model by Landau and Lifshitz.** The foundation of magnetization precession is laid by quantum mechanics, where the mean value of the spin operator S evolves according to Schrödinger's equation,

$$\frac{d}{dt}\langle S\rangle(t) = \frac{g\mu_B}{h}\langle S\rangle(t) \times B(t)\,,$$

and $B(t) = \mu_0 H(t)$. If the magnetization $m : \omega \to S^2$ is understood to be the dipole of spins per unit volume we arrive at the Landau-Lifshitz equation (LL), governing magnetization motion

$$m_t(t) = \gamma_0\, m(t) \times H(t)\,. \tag{3.1}$$

Assuming the magnetic field to be time independent, successive multiplication by m and H leads to

$$\frac{d}{dt}|\, m(t)\,|^2 = 0\,, \qquad \frac{d}{dt}\langle m(t), H\rangle = 0\,.$$

Hence, the modulus of the magnetization remains unchanged during motion, and the angle between the magnetization also remains constant as a function of time. Landau-Lifshitz therefore describes a precessional motion of the magnetization around the applied field, as sketched in Figure 3, and the angular frequency is a linear function of the magnetic field, $\omega_0 = \gamma_0|\, H\,|$. The possibility of infinitely fast precession in finite time is evidenced by the following example (from [26]).

Example 3.1. *Let $a, m_0 \in \mathbb{R}^3$. Then the unique solution of $m_t(t) = a \times m(t)$, $t > 0$, for $m(0) = m_0$ is given by the unimodular evolution*

$$m(t) = \exp(at) \times m_0 = m_0^{\parallel} + m_0^{\perp}\cos\big(|\, a\,|t\big) + \frac{a}{|\, a\,|} \times m_0^{\perp}\sin\big(|\, a\,|t\big)\,,$$

for $m_0 = m_0^{\perp} + m_0^{\parallel}$, where $m_0^{\parallel}$ is parallel to a, and $m_0^{\perp}$ is perpendicular to a.

From a mathematical viewpoint, it is only recently that solution concepts have been studied for (LL) in the form $m_t = m \times \Delta m$, for $m : \omega \to S^2$, and $\omega \subset \mathbb{R}^2$. Existence of weak solutions to the related Cauchy problem goes back to [93], and global existence of smooth solutions for small initial energies ($n = 2$) is studied in [21, 93]; an open question is on existence of a global smooth solution of (LL) for $n \geq 2$. In [48], B. Guo, Y. Han, and G. Yang construct the solution $m(r,t) = -\frac{1}{r^2}\big(\frac{1}{4}, \cos(\frac{r^4}{4(T-t)}), \sin(\frac{r^4}{4(T-t)})\big)$, $0 \leq t < T$ of the 2D cylindrical symmetric Landau-Lifshitz equation $m_t = m \times m_{rr} + \frac{1}{r} m \times m_r$ showing finite-time blow-up, i.e., $\lim_{t\to T-} \|\, \nabla m\,\|_{L^\infty(\omega,\mathbb{R}^6)} = \infty$; see also [70] in this context. So far, it is known for (LL) that as long as $\|\, \nabla m\,\|_{L^\infty(\omega,\mathbb{R}^{3n})}$ is bounded, then the solution remains regular for all times, so singularities are indicated by loss of control on $\|\, \nabla m\,\|_{L^\infty(\omega,\mathbb{R}^{3n})}$; this statement is based on the energy identity, which gives a bound for $\|\, \nabla m\,\|_{L^2(\omega,\mathbb{R}^{3n})}$.

Singularities also play an important role in establishing uniqueness of solutions; in particular, when the singularities are weak enough, solutions can be extended in a weak sense beyond the singularity, possibly in a non-unique fashion. The question of whether weak solutions are unique is not known for the two-dimensional (LL); there are different characterizations of weak solutions, and it is not clear whether they coincide. For the related equations of harmonic map heat flow and wave maps, there exist non-unique solutions due to the appearance of singularities [30].

¿From a physical viewpoint, the mathematical concept of singularities translates to defects and spatial energy concentration in ferromagnetic materials. The issue of nonuniqueness is important for micromagnetic simulation. Understanding the source and characterizing the nature of singularities affects issues involving the validity of the physical model as well as what allowable features should be present in the definition of weak solution.

Another well-known approach to studying (LL) and its possible singularities rewrites the problem as a perturbed version of cubic nonlinear Schrödinger equation by stereographically projecting the target sphere S^2 onto the complex plane, $q_t = i\Delta q + \partial^{-1}(|\, q^2\,|^2)\partial q + \mathcal{O}(q^3)$. Main motivations of this approach are

(1) equivalence of $m_t = m \times m_{xx}$ with the cubic nonlinear Schrödinger equation $q_t = i(q_{xx} + |\, q\,|^2 q)$ in one space dimension, using Hasimoto transform.

(2) extensive results available on solution's behavior for the cubic nonlinear Schrödinger equation $q_t = i(\Delta q - |\, q\,|^2 q)$ in higher dimensions: for $n < 2$, no singularities appear, whereas singularities can form in the critical and supercritical cases $n \geq 2$. These studies heavily benefit from the underlying principles of conservation of $\|\, q\,\|_{L^2}$ — i.e., multiply by $\overline{q}$ and take real part —, and energy $E(q) = \frac{1}{2}\int_\omega |\, \nabla q\,|^2\, \mathrm{d}x - \frac{1}{4}|\, q\,|^4\, \mathrm{d}x$ — i.e., multiply by $\overline{q}_t$ and take imaginary part.

Unfortunately, part of the analytical methods which are used to study blow-up behavior of solutions to cubic nonlinear Schrödinger equation fail in the context of (LL), which motivates numerical studies instead; see [58].

3.1.1. *Discretization of Landau-Lifshitz equation.* It is due to the highly nonlinear character of $m_t = m \times \Delta m$ that explicit time integrators is often given preference over implicit ones. However, only high-order explicit

discretizations possess nontrivial stability regions in this case, as detailed in [101]; the following observation is taken from this reference.

Example 3.2. *Let $a, m_0 \in \mathbb{R}^3$. The discretization of the problem $m_t(t) = a \times m(t)$, $t > 0$, for $m(0) = m_0$ by explicit Euler reads*

$$m^{j+1} = m^j - k\, a \times m^j \equiv A m^j\,, \qquad m^0 = m_0\,.$$

The three eigenvalues of A are $\lambda_1 = 1$, $\lambda_2 = 1 + |a|ki$, $\lambda_3 = 1 - |a|ki$, hence $\rho(A) = \sqrt{1 + |a|^2 k^2} > 1$. This implies that the stability region for the Euler scheme contains only $\{k = 0\}$.

This observation results from the fact that stability regions of the explicit Euler method do not contain any part of the imaginary axis except the origin. On the other hand, the stability regions of the classical third- and fourth-order Runge-Kutta schemes do contain part of the imaginary axis. For example, absolute stability of the fourth-order explicit Runge-Kutta scheme to solve $m_t(t) = a \times m(t)$, $m(0) = m_0$ holds for cases $k = \mathcal{O}(\frac{1}{|a|})$, see [101]. This shortcoming of explicit first-order method can be cured by artificially injected dissipative mechanisms during the computation. One possibility is a semi-implicit (Gauss-Seidel) strategy, yielding to absolute stability for choices $k = \mathcal{O}(\frac{1}{|a|})$. If applied to $m_t(t) = m(t) \times \Delta m(t)$, the following semidiscretization in time is proposed in [101] to compute iterates $\{m^j\}_{1 \le j \le J}$, for $m^j = (m_1^j, m_2^j, m_3^j)$.

Algorithm 3.1. *1. Let $m^0 = m_0$.*
2. Given m^j, $0 \le j \le J$, find m^{j+1} that solves

$$\begin{pmatrix} m_1^{j+1} \\ m_2^{j+1} \\ m_3^{j+1} \end{pmatrix} = \begin{pmatrix} m_1^j + k\,(m_3^j \Delta m_2^j - m_2^j \Delta m_3^j) \\ m_2^j + k\,(m_1^{j+1} \Delta m_3^j - m_3^j \Delta m_1^{j+1}) \\ m_3^j + k\,(m_2^{j+1} \Delta m_1^{j+1} - m_1^{j+1} \Delta m_2^{j+1}) \end{pmatrix}.$$

An implicit variant of this scheme is discussed in [101] as well, and computational experiments motivate its unconditional stability.

A different strategy to obtain a convergent discretization of (LL) is realized in [9], where (LL) is approximated by Landau-Lifshitz-Gilbert equation (3.2), for $H_{\text{eff}} = \Delta m$; this approach uses artificial additional damping which comes from the term headed by $\alpha_1 > 0$. For choices $\alpha_1 = ch^2$, and $k = \mathcal{O}(h^2)$, convergence on quasiuniform meshes $\mathcal{T}_h$ of Algorithm 3.3 can be verified. The following example is taken from [9].

Example 3.3. *Let $H_{\text{eff}} = \Delta m$, $\alpha_2 = 1$, and $\omega = (-0.5, 0.5)^2$. Choose initial data $m_0 \in L^\infty(\omega, S^2)$ as*

$$m_0(x,y) = \begin{cases} (0,0,-1) & \text{for } r > \frac{1}{2} \\ \frac{1}{a^2+r^2}(2ax, 2ay, a^2 - r^2) & \text{for } r \le \frac{1}{2} \end{cases}$$

for $r = r(x,y) = \sqrt{x^2 + y^2}$, and $a = a(x,y) = (1 - 2r)^4$. Figure 11 explains finite-time blowup as simultaneous accelerated precession around x_3-axis (given by angle $-\pi < \theta \le \pi$), and switching the direction (given by angle $-\frac{\pi}{2} \le \phi \le \frac{\pi}{2}$); cf. also Figure 3 (a). Note that the energy identity $\frac{d}{dt} I(m,t) = 0$ is valid throughout the experiment, where $I(m,t) = \int_0^t \| m_t(s) \|^2 \, \mathrm{d}s + \frac{1}{2} \| \nabla m(t) \|^2$.

Hysteresis curves usually tell us that beyond some value of the applied field, any magnetic sample can be considered saturated. The magnetization is then uniform and aligned with the field. Precession alone does not allow us to reach that limit, in contradiction to experimental evidence. Therefore, the precession equation has to include a damping term so that, after some finite time, the magnetization become aligned with the applied field. By far, the simplest way of introducing a damping term to (3.1) consists of replacing the field H by an effective field including an ohmic type dissipation term, $H_{\text{eff}} = H - \frac{\alpha}{\gamma_0 M_s} m_t$, where M_s is the saturation magnetization and $\alpha > 0$ a phenomenological damping parameter. One also often refers to Rayleigh type dissipation because the associated dissipation function is a combination of the generalized velocities squared. We then obtain the Landau-Lifshitz-Gilbert (LLG) equation

$$m_t(t) = \gamma_0\, m(t) \times H(t) - \frac{\alpha}{M_s}\, m(t) \times m_t(t)\,.$$

The effect of damping is illustrated in Figure 3 (b): as time passes, the magnetization spirals down until it becomes aligned with the field, and all torques acting on m then vanish. The study of (LLG) is the subject of the subsequent section.

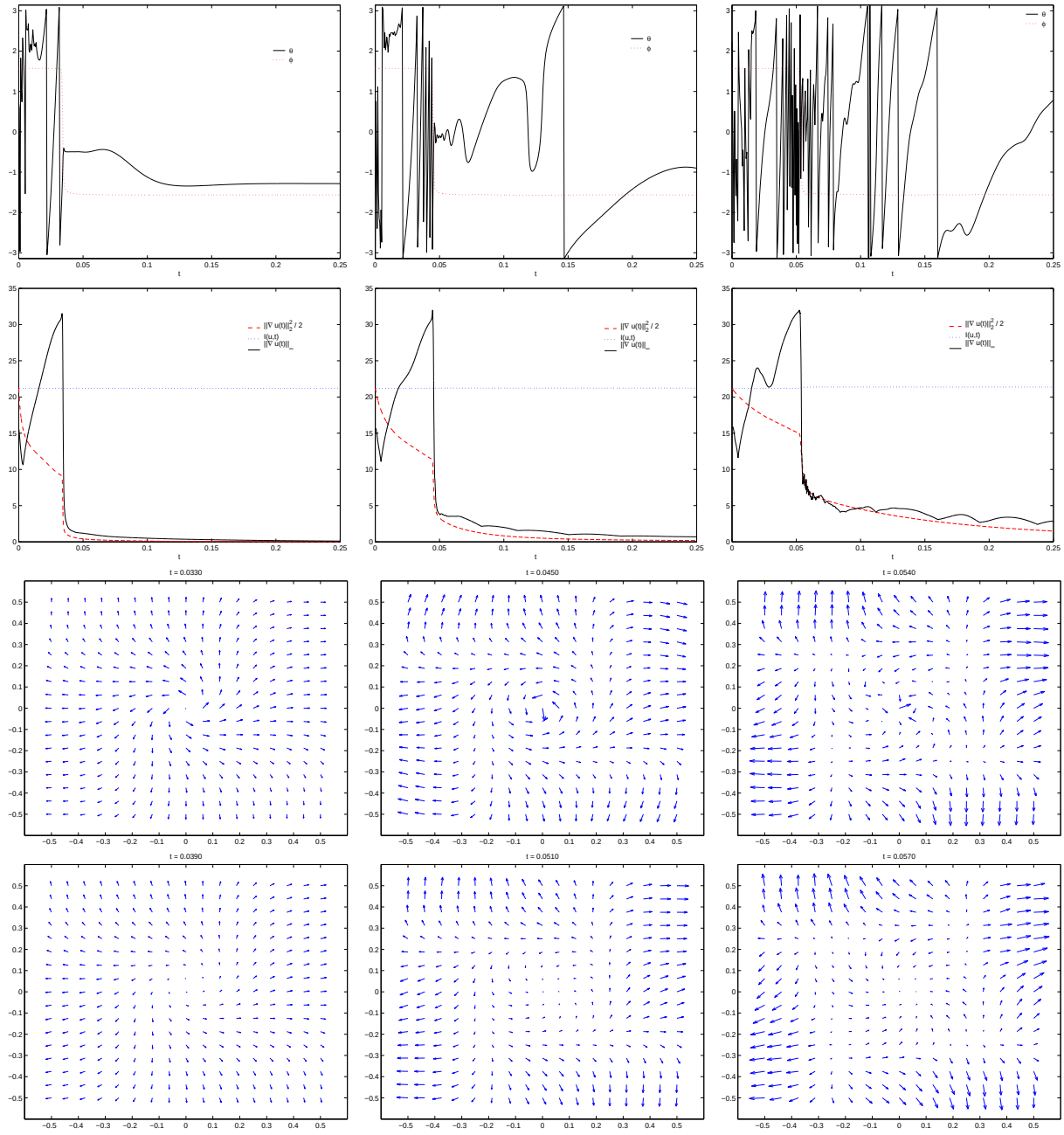

FIGURE 11. Accelerated, switched precession at $(0,0)$ (1st row), corresponding plots for $\frac{1}{2}\|\nabla m\|_2^2$ vs. $\|\nabla m(0,0)\|_{\mathbb{R}^6}$ (2nd row), and magnetization patterns shortly before (3rd row) and after (4th row) blowup time, for different damping parameters $\alpha_1 = 1, \frac{1}{4}, \frac{1}{16}$ (columnwise) (from [9]).

3.2. **The model by Landau, Lifshitz and Gilbert.** When the effective magnetic field H_{eff} varies in time, the configuration (m,u) eventually may start to evolve too. Depending on considered scales, different models are used to describe highly nonlinear phenomena: at a microscopic level, Landau-Lifshitz-Gilbert model is used to describe evolution of domains and structured domain walls (Bloch walls, Neel walls, cross-tie walls, etc.) or codimension-2 defects called vortices in thin films; although small in dimension, they enforce a nontrivial topological arrangement of the magnetization field. Spin dynamics ('magnetization

reversal') from millisecond down to femtosecond timescales in magnetic materials of micrometers down to dozens of nanometers is the key for fast data storage in hard disks. One certain disadvantage of the model is that it describes evolution of pronounced microstructures rather than averaged magnetic properties; hence, phenomenological rate-independent models motivated from those in plasticity theory are used to describe magnetization dynamics on a mesoscopic level, as will be further detailed in Section 3.3.

The Landau-Lifshitz-Gilbert equation [68] describes the evolution of spin fields in continuum ferromagnets around the effective field $H_{\rm eff}$,

$$m_t = -\alpha_1\, m \times (m \times H_{\rm eff}) + \alpha_2\, m \times H_{\rm eff}\,, \quad \alpha_1, \alpha_2 \geq 0\,, \tag{3.2}$$

where $m \equiv (m^1, m^2, m^3) : \omega \times (0,T) \to \mathbb{R}^3$, with $|\, m\,| = 1$, and $H_{\rm eff} = -D\mathcal{E}_\alpha$, together with (1.4), and Maxwell's equation (1.1) in a quasistatic approximation. This equation linearly combines the heat flow of harmonic maps to the sphere S^2, $m_t = -m \times (m \times \Delta m)$, and the Schrödinger flow $m_t = m \times \Delta m$ in the case $\overline{H}_{\rm eff} = \Delta m$.

Problem (3.2) is a strongly coupled degenerated quasilinear parabolic system which makes it hard to analyze mathematically. In order to understand essential properties of this phenomenological model describing nonequilibrium magnetism, we restrict to exchange energy contributions in the effective field, defining thus the reduced effective field $\overline{H}_{\rm eff} = \Delta m$. Supposing classical solutions to (3.2) in this case, by using the identity $a \times (b \times c) = \langle a, c\rangle_{\mathbb{R}^3} b - \langle a, b\rangle_{\mathbb{R}^3} c$, we compute

$$m \times (m \times \Delta m) = \langle m, \Delta m\rangle_{\mathbb{R}^3} m - |\, m\,|^2 \Delta m\,.$$

In addition, if we multiply (3.2) by m, we find $\langle m, m_t\rangle_{\mathbb{R}^3} \equiv \frac{1}{2}\frac{d}{dt}|\, m\,|^2 = 0$, and hence $|\, m\,|^2 = 1$, everywhere in $\mathbb{R}^+ \times \omega$. Now, $m \cdot \nabla m = 0$, or $\langle m, \Delta m\rangle_{\mathbb{R}^3} = -|\, \nabla m\,|^2$, which is the reason for the following Landau-Lifshitz-Gilbert (LLG) equation

$$m_t - \alpha_1\, \Delta m = \alpha_1\, |\, \nabla m\,|^2 m + \alpha_2\, m \times \Delta m \quad \text{in } \omega_T := (0,T) \times \omega\,, \tag{3.3}$$

$$\partial_n m = 0 \quad \text{on } \partial\omega_T := (0,T) \times \partial\omega\,, \tag{3.4}$$

$$m(0,x) = m_0(x) \quad \forall\, x \in \omega\,, \quad |\, m_0\,| = 1 \quad \text{a.e. in } \omega\,. \tag{3.5}$$

Note that the natural boundary condition resulting from balance of torque, $m \times \partial_n m = 0$ can be simplified to (3.4) as $m \in S^2$. — If (3.3) holds in a classical sense, an equivalent formulation would result from taking the cross-product with m to replace the term scaled by α_2,

$$\frac{\alpha_1}{\alpha_1^2 + \alpha_2^2} m_t - \frac{\alpha_2}{\alpha_1^2 + \alpha_2^2} m \times m_t = \Delta m + |\, \nabla m\,|^2 m \quad \text{in } \omega_T\,, \tag{3.6}$$

which is also known as Gilbert equation [44]. By again using the above vector identity and $|\, m\,|^2 = 1$, it can be recast into the form

$$\frac{\alpha_2}{\alpha_1^2 + \alpha_2^2} m_t + \frac{\alpha_1}{\alpha_1^2 + \alpha_2^2} m \times m_t = m \times \Delta m \quad \text{in } \omega_T\,. \tag{3.7}$$

The choice between the Gilbert version and the Landau-Lifshitz version of the dynamic equation for magnetization is often based on mathematical convenience; both equations preserve the length of a smoothly varying magnetization vector and both can be studied in the framework of evolution problems of harmonic maps. — The subsequent example is taken from [85].

Example 3.4. *In* [100]*, the Landau-Lifshitz solution of Example 2.1 is generalized to the nonstationary case, where* $H_{\rm ext} = -H\xi_3$ *is aligned to the easy axis, and* $H < \frac{\alpha_1}{2\alpha_2}$ *constant is not too big. The traveling-wave solution found by Walker is*

$$\vartheta(x_1,t) = \arccos\big(\tanh\frac{x_1 - v_H t}{\delta_H}\big)\,, \qquad \varphi(x_1,t) = \varphi_H\,,$$

for fixed $(\,\varphi_H, \delta_H, v_H\,)$ *given by*

$$\sin(2\varphi_H) = -\frac{2\alpha_2}{\alpha_1} H\,, \qquad \delta_H = \sqrt{\frac{\alpha}{\beta \sin^2(\varphi_H)}}\,, \qquad v_H = H\frac{\alpha_1^2 + \alpha_2^2}{\alpha_2}\sqrt{\frac{\alpha}{\beta + \sin^2(\varphi_H)}}\,.$$

The solution supports the idea of a flat domain wall moving with velocity v_H in a direction of the x_1-axis. Hence, crucial parameters which control the dynamics of a domain wall are its thickness w and wall mobility $\nu := \lim_{H\to 0} \frac{v_H}{H} = \frac{w(\alpha_1^2+\alpha_2^2)}{\alpha_2}$.

First existence results for (LLG) also in the presence of magnetostrictive effects are due to Visintin [97], see also [12]: locally existing solutions are globally extended thanks to the valid energy law, see below. In 1992, by a method introduced in [30] to prove nonuniqueness of weak solutions to the heat flow of harmonic maps, Alouges and Soyeur [5] established a nonuniqueness result for weak solutions to problem (3.3)–(3.5) for $\omega \subset \mathbb{R}^3$; the idea is to take a singular solution of the type $g(\frac{x}{|x|})$ as the initial datum, and then to show that there is another nonstatic solution emanating from such a datum. These earlier results do not discuss possible singularities of the solution, which is provided by a further study of weak solutions ('Struwe solutions') for domains $\omega \subset \mathbb{R}^2$ without boundary due to Guo and Hong [45]: these solutions are regular away from at most finite many isolated points in ω_T, and with decreasing energy; they are globally regular in the case of small initial energies. Their proof uses the intrinsic Liapunov structure of the problem, and local energy arguments developed for harmonic maps by Struwe, see [92] for a survey. In the sequel, study of partial regularity of Struwe solutions [38] and their uniqueness [22] (cf. [50] for correcting remarks) again follow corresponding previous results in the harmonic mapping theory (1994 M. Feldman, 1995 Y. Chen, J. Li, F.H. Lin, 2002 R. Moser on partial regularity of Struwe's solution, and 1996 A. Freire on uniqueness of Struwe's solution for 2D-Cauchy problem).

Definition 3.1. *A vector function $\{m(t,x)\}$ is said to be a global weak solution to* (3.6)*, if m is defined a.e. in ω_T such that*

(1) $m \in L^\infty(0,\infty; H^1(\omega,\mathbb{R}^n))$ *and* $m_t \in L^2((0,\infty); L^2(\omega,\mathbb{R}^n))$,
(2) $|\, m(t,x)\,|^2 = 1$ *a.e. on* $\mathbb{R}^+ \times \omega$,
(3) (3.6) *holds in the sense of distributions,*
(4) $m(0,x) = m_0(x)$ *in the sense of traces,*
(5) *for all* $T > 0$,

$$\frac{1}{2} \| \nabla m(T) \|^2 + \frac{\alpha_1}{\alpha_1^2+\alpha_2^2} \int_0^T \| m_t(s) \|^2 \, \mathrm{d}s \le \frac{1}{2} \| \nabla m_0 \|^2 .$$

Verification of weak solutions to (LLG) in higher dimensions requires a Ginzburg-Landau penalization strategy [45, 92], which defines a weak solution m to (LLG) as suitable limit of $\{m^\varepsilon\}_{\varepsilon>0}$, where each element solves

$$\frac{\alpha_1}{\alpha_1^2+\alpha_2^2} m_t^\varepsilon - \frac{\alpha_2}{\alpha_1^2+\alpha_2^2} m^\varepsilon \times m_t^\varepsilon - \Delta m^\varepsilon + g(m^\varepsilon) = 0 \quad \text{in } \omega_T , \tag{3.8}$$

$$\frac{\partial m^\varepsilon}{\partial n} = 0 \quad \text{on } \partial\omega_T , \tag{3.9}$$

$$m^\varepsilon(0,x) = m_0^\varepsilon(x) \quad \forall\, x \in \omega , \quad |\, m^0\,| = 1 \quad \text{in } \omega , \tag{3.10}$$

for $g(m^\varepsilon) = \nabla G(m^\varepsilon)$, and $G(m^\varepsilon) = \frac{1}{4\varepsilon^2}(|\, m^\varepsilon\,|^2 - 1)^2$; by standard Galerkin approximation, consider solutions $\{m^{\varepsilon,h}\}$ which satisfy the (semi-)discrete energy identity

$$\frac{\alpha_1}{\alpha_1^2+\alpha_2^2} \int_0^T \| m_t^{\varepsilon,h}(s) \|^2 \, \mathrm{d}s + \frac{1}{2} \| \nabla m^{\varepsilon,h}(T) \|^2 + \int_0^T \int_\omega G(m^{\varepsilon,h}) \, \mathrm{d}x\mathrm{d}s = \frac{1}{2} \| \nabla m_0 \|^2 , \qquad h > 0 , \tag{3.11}$$

where h is a mesh parameter. This result carries over to the limiting case $h \to 0$; moreover, by testing (3.8) with $m^\varepsilon - \frac{m^\varepsilon}{|\, m^\varepsilon\,|} \min\{1, |\, m^\varepsilon\,|\}$ one may show $|\, m^\varepsilon\,| \le 1$, a.e. on $\mathbb{R}^+ \times \omega$. Both ingredients now suffice to select convergent subsequences (not relabeled) $\{m^\varepsilon\}_\varepsilon$ such that

$$\begin{aligned}
&m^\varepsilon \to m \quad \text{weakly* in } L^\infty\big(\mathbb{R}^+; H^1(\omega,\mathbb{R}^n)\big) , \\
&m_t^\varepsilon \to m_t \quad \text{weakly in } L^2\big(\mathbb{R}^+; L^2(\omega,\mathbb{R}^n)\big) , \\
&m^\varepsilon \times m_t^\varepsilon \to m \times m_t \quad \text{weakly in } L^2\big(\mathbb{R}^+; L^2(\omega,\mathbb{R}^n)\big) \\
&m^\varepsilon \to m \quad \text{strongly in } L^2\big(\mathbb{R}^+; L^2(\omega,\mathbb{R}^n)\big) , \\
&|\, m\,| = 1 \quad \text{a.e. on } \mathbb{R}^+ \times \omega .
\end{aligned} \tag{3.12}$$

Finally, by taking the cross-product of (3.8) with m^ε, we can verify that the limit satisfies (3.6).

Remark 3.1. *For the Cauchy problem $\omega = \mathbb{R}^3$, Alouges & Soyeur [5] use a finite difference discretization of (3.2) ($\tilde{H}_{\rm eff} = \Delta m$) to derive the following ODE with Lipschitz-continuous right-hand side,*

$$\partial_t m_h = -\alpha_1\, m_h \times (m_h \times \tilde{\Delta}_h m_h) + \alpha_2\, m_h \times \tilde{\Delta}_h m_h\,, \qquad m_h(0) = m_{0,h}\,,$$

This identity holds for all grid-points, where $\tilde{\Delta}_h$ denotes the standard discrete Laplacian; conservation of $|\, m_h\,| = 1$ at every grid-point and a semi-discrete energy law are the relevant steps to verify existence of a weak solution in this context.

Remark 3.2. *An interesting approach to understand wall dynamics is given in [85], where a reduced sharp-interface model for their dynamics in hard ferromagnetic bodies is derived from (LLG) by asymptotic analysis ($\beta \to \infty$). The idea of the construction is to asymptotically balance wall thickness, anisotropy effects, and wall mobility appropriately, leading to a limiting equation which describes evolution of the flat domain wall by its mean curvature and a nonlocal forcing term.*

A crucial problem in the analysis of (3.2) is again the nonconvex constraint $|\, m\,| = 1$, which is penalized by Ginzburg-Landau approximation (3.8); perturbation effects due to this strategy are then controlled by stability properties (i.e., energy law, and $|\, m^\varepsilon\,| \le 1$) to eventually verify convergence (3.12). Next to the strongly nonlinear character of the problem, proper dealing with the nonconvexity numerically is a problem since it cannot be satisfied a.e. anymore. Explicit time integrators of high order and occasional updates during the evolution to approximate $|\, m\,| = 1$ are most commonly used strategies in engineering literature [42], which suffer from severe limitations with respect to admissible time steps [40, 101], and non-reliable dynamics. From this perspective, recent developments in numerical micromagnetism aim at constructing efficient convergent schemes for the cases $H_{\rm eff} = -D\mathcal{E}_\alpha$, both for $\alpha = 0$ and $\alpha > 0$. First results for the case $\alpha = 0$ in the more general framework of Maxwell-(LLG) have been done by Joly, Vacus, and Monk [54, 53, 78], addressing energy decay and conservation of length for iterates of their proposed schemes in the case of (known) smooth driving (electro-)magnetic fields. Approaches base on the given form (3.2) to easily detect these stability properties in the discrete setting. An interesting, semidiscrete scheme to efficiently solve (3.2) is proposed in [26]:

Algorithm 3.2. *1. Let $m^{0,\ell} = m_0$, for $\ell \ge 0$.*
2. For each $1 \le j \le J$, $1 \le \ell \le \ell_{j,\max}$, and $m^{j,0} = m^{j-1,\ell_{j-1,\max}}$, compute $m^{j,\ell} \in L^\infty(\omega, \mathbb{R}^n)$ from

$$d_t m^{j,\ell} = -\frac{\alpha_1}{4}\frac{m^{j,\ell}}{|\, m^{j,\ell}\,|} \times \Big(\big(m^{j-1,\ell-1} + m^{j,\ell-1}\big) \times \big(H_{\rm eff}^{j-1,\ell-1} + H_{\rm eff}^{j,\ell-1}\big)\Big) + \alpha_2\, m^{j,\ell} \times \big(H_{\rm eff}^{j-1,\ell-1} + H_{\rm eff}^{j,\ell-1}\big)\,.$$

3. Stop iteration at level $1 \le j \le J$ in case $|\, m^{j,\ell} - m^{j,\ell-1}\,| \le k^\beta$, $\beta > 0$, and set $m^{j,\ell} = m^{j-1,\ell_{j-1,\max}}$.

For smooth $H_{\rm eff} = -D\varphi + H$, $\beta \ge 3$ and $k \le k_0(t_J)$ this is a second order convergent, length-preserving method [26]; in practice, $\max_j \ell_{j,\max} = 2$ is usually sufficient to meet the stopping criterion. In the remainder of this subsection, we now focus on the case $\alpha > 0$.

3.2.1. *Discretization of Ginzburg-Landau penalization* (3.8)–(3.10). In [83], Pistella & Valente studied finite-time blow-up of solutions to (LLG) subjected to additional surface exchange contributions numerically: for this purpose, they consider a fully discrete finite-difference version of the Ginzburg-Landau approximation ($\alpha_1, \alpha_2 \ge 0$)

$$m_t^\varepsilon - \alpha_1\, \Delta m^\varepsilon + \alpha_1 g(m^\varepsilon) = \alpha_2\, (m^\varepsilon \times \Delta m^\varepsilon) \quad \text{in } \omega_T\,, \tag{3.13}$$

$$\partial_n m^\varepsilon = 0 \quad \text{on } \partial\omega_T\,, \tag{3.14}$$

$$m^\varepsilon(0,x) = m_0(x) \quad \forall\, x \in \omega\,, \quad |\, m_0\,| = 1 \quad \text{in } \omega\,, \tag{3.15}$$

for $g = \nabla G$, with $G(x) = \frac{1}{4\varepsilon^2}(x^2-1)^2$, which is based on explicit Euler's method; by restricting the time-step $k > 0$ as follows ($\alpha_1 = \alpha_2 = 1$),

$$k \le \min\Big[\frac{\varepsilon^2 h^2}{2(\varepsilon^2 + h^2)}, \frac{h^2}{4}\Big]\,, \tag{3.16}$$

$\max_i |\, m_h^{\varepsilon,j}\,| \le 1$ and a discrete energy-law corresponding to (3.11) are verified. These stability results are the key to verify convergence of a subsequence to solutions of (3.13)–(3.15), for every positive $\varepsilon > 0$, and

finally of a subsequence to the weak solution of the limiting problem (3.3); see also [20] for blow-up studies using a stable, semi-explicit finite-difference scheme to discretize the limiting problem (3.7) directly.

Approximation of structures governed by (LLG) requires small values of $\varepsilon > 0$, such that (3.16) severely restricts values of time-steps $k > 0$. From this point of view, the following discretization of (3.8)–(3.10) is more flexible (cf. e.g., [41]): Given $m_{0,h} = P_h m_0$, find $m_h^j \in V_h(\omega; \mathbb{R}^n)$ for all $1 \le j \le J$ such that

$$\begin{aligned} &\frac{\alpha_1}{\alpha_1^2+\alpha_2^2}\Big(d_t m_h^j, \phi_h\Big) + \Big(\nabla \overline{m}_h^{j-1/2}, \nabla \phi_h\Big) \\ &+\frac{1}{2\varepsilon^2}\Big((|\, m_h^j\,|^2 + |\, m_h^{j-1}\,|^2 - 2)\overline{m}_h^{j-1/2}, \phi_h)\Big) = \frac{\alpha_2}{\alpha_1^2+\alpha_2^2}\Big(m_h^{j-1} \times d_t m_h^j, \phi_h\Big)\,, \end{aligned} \tag{3.17}$$

where we denote $d_t\phi^j := k^{-1}\{\phi^j - \phi^{j-1}\}$ and $\overline{\phi}^{j-1/2} := \frac{1}{2}\{\phi^j + \phi^{j-1}\}$. Note that the right-hand term in (3.17) comes in a linear form, since $(\overline{m}_h^{j-1/2} \times d_t m_h^j, \phi_h) = (m_h^j \times d_t m_h^j, \phi_h)$. Consistency and discrete energy law are desirable characteristics of (3.17) for the whole range of parameters $k, h, \varepsilon > 0$.

Lemma 3.1. *The solution $\{m_h^j\}_{j=1}^J$ satisfies for any $k > 0$*

(i) $\quad \|\, m_h^j \,\|_{L^\infty} \le 1\,,$

(ii) $\quad \dfrac{\alpha_1}{\alpha_1^2+\alpha_2^2} k \sum_{j=1}^{J} \|\, d_t m_h^j \,\|^2 + \dfrac{1}{2} \max\limits_{1\le j\le J} \|\, \nabla m_h^j \,\|^2 + \|\, G(m^j) \,\|_{L^1} = \dfrac{1}{2} \|\, \nabla m_{0,h} \,\|^2\,.$

Proof. Choosing $\phi_h = d_t m_h^{j+1}$ yields the result. □

3.2.2. *Approximation of weak solutions to (LLG).* As outlined in Section 3.2, so far it is not clear whether (3.2) also admits finite-time singularity formation. For this reason, it is convenient that reliable numerics for (LLG) has to deal with weak solutions. Verification of a corresponding discrete energy law for a discretization of the limiting problem (3.2) ($H_{\text{eff}} = \Delta m$) is a challenging task: first, conservation of $|\, m\,| = 1$ rules out the implicit Euler method; second, spatial discretization using finite elements does not allow this nonconvex constraint to hold in a pointwise fashion.

Example 3.5. *Given $m_0 \in H^1(\omega, S^{n-1})$, consider the implicit Euler method*

$$d_t m^j - \alpha_1\, \Delta m^j \;=\; \alpha_1\, |\, \nabla m^j\,|^2 m^j + \alpha_2\, m^j \times \Delta m^j \quad \text{in } \omega\,, \qquad \frac{\partial m^j}{\partial n} = 0 \quad \text{on } \partial\omega\,.$$

We proceed by contradiction, and suppose $|\, m^j\,| = 1$ almost everywhere: multiplication with m^j yields

$$d_t |\, m^j\,|^2 + k\, |\, d_t m^j\,|^2 = 0 \quad \text{for a.e. } x \in \omega\,.$$

Note that $|\, m^j\,|^2 = 1$ a.e. in ω is violated in general — in contrast to the continuous equation.

We now propose two fully discrete, consistent schemes which satisfy a discrete energy law and hence allow for approximation of weak solutions to (LLG).

The first scheme uses lumped mass integration defined by

$$(\chi, \eta)_h = \sum_{K\in\mathcal{T}_h} \int_K I_h(\chi\eta)\,\mathrm{d}x \quad \forall\, \chi, \eta \in C(\overline{\omega})\,,$$

where $I_h : C(\overline{\omega}) \to V^h$ denotes the (linear) Lagrange interpolation operator on $\mathcal{T}_h$.

The following first discretization of (3.2) is consistent.

Problem 3.1. *Given $m_h^0 = I_h(m^0)$, compute iterates $m_h^j \in V_h(\omega; \mathbb{R}^n)$, $j \ge 1$ from*

$$\begin{aligned} (d_t m_h^j, \phi_h)_h \;=\; &-\alpha_1\big(\overline{m}^{j+1/2} \times (\overline{m}^{j+1/2} \times \Delta_h \overline{m}^{j+1/2}), \phi_h\big) \\ &+\alpha_2\big(\overline{m}_h^{j+1/2} \times \Delta_h \overline{m}_h^{j+1/2}), \phi_h\big) \quad \forall\, \phi_h \in V_h(\omega; \mathbb{R}^n)\,. \end{aligned}$$

Here, we denote $(-\Delta_h\phi_h, \mathfrak{Z}_h) = (\nabla\phi_h, \nabla\mathfrak{Z}_h)$. By Lipschitz-continuity of the right-hand side, the problem has a unique solution. The following bounds verify $|\, m_h^j(x)\,| = 1$ for all vertices $x \in \mathcal{E}$, as well as discrete energy law for (3.18) for every $k > 0$, and every $1 \le j \le J$,

$$\text{(i)} \qquad |\, m_h^j(x)\,| = 1 \quad \forall\, x \in \mathcal{E}\,,$$

$$\text{(ii)} \qquad \frac{1}{2}\|\, \nabla m_h^J\,\|^2 + \alpha_1 k \sum_{j=1}^{J} \|\, \overline{m}_h^{j+1/2} \times \Delta_h \overline{m}_h^{j+1/2}\,\|^2 = \frac{1}{2}\|\, \nabla m_h^0\,\|^2\,.$$

Verification follows from choosing $\phi_h = \phi_i \overline{m}_h^{j+1/2}$, $\phi_i \in V_h(\omega, \mathbb{R}^2)$ such that $\phi_i(x_\ell) = \delta_{i\ell}$ to verify (i); assertion (ii) follows from selecting $\phi_h = -\Delta_h \overline{m}_h^{j-1/2}$. However, convergence towards weak solutions of (3.3)–(3.5) is an open problem.

Another discretization of (LLG) is due to Alouges & Jaisson [4] and uses the Gilbert equation (3.7): if we take $\phi = m \times w$, where $w \in H^1(\omega_T, \mathbb{R}^3) \cap L^\infty(\omega_T, \mathbb{R}^3)$ satisfies $\langle w, m\rangle_{\mathbb{R}^3} = 0$ a.e. in ω, we get

$$\begin{aligned} \frac{\alpha_1}{\alpha_2}\int_{\omega_T} \langle m_t, w\rangle_{\mathbb{R}^3}\,\mathrm{d}x\mathrm{d}t \;&-\; \int_{\omega_T} \langle m \times m_t, w\rangle_{\mathbb{R}^3}\,\mathrm{d}x\mathrm{d}t \\ &= -\frac{\alpha_1^2+\alpha_2^2}{\alpha_2}\int_{\omega_T} \langle \nabla m, \nabla w\rangle_{\mathbb{R}^9}\,\mathrm{d}x\mathrm{d}t\,, \end{aligned} \tag{3.18}$$

from which the original weak formulation is re-obtained by taking $w = m \times \phi$, for any $\phi \in C_0^\infty(\omega_T, \mathbb{R}^n)$.

Now, consider the following subsets of $V_h(\omega; \mathbb{R}^n)$,

$$\begin{aligned} \mathcal{M}_h &= \big\{\phi_h \in V_h(\omega;\mathbb{R}^n)\big|\, |\,\phi_h(x_\ell)\,| = 1\ \forall\, x_\ell \in \mathcal{E}\big\}\,, \\ \mathcal{F}_h^j &= \big\{\phi_h \in V_h(\omega;\mathbb{R}^n)\big|\, \langle w(x_\ell), m_h^j(x_\ell)\rangle_{\mathbb{R}^3} = 0\ \forall\, x_\ell \in \mathcal{E}\big\} \qquad \forall\, m_h^j \in \mathcal{M}_h\,. \end{aligned}$$

A discretization of (3.18) could be obtained via the following Crank-Nicolson procedure: Let $m_h^0 = P_0 m_0$. For $m_h^j \in \mathcal{M}_h$ being given, find $m_h^{j+1} \in \mathcal{M}_h$ that solves for all $w_h \in \mathcal{F}_h^{j-1}$:

$$\frac{\alpha_1}{\alpha_2}(d_t m_h^j, w_h) - (m_h^{j-1} \times d_t m_h^j, w_h) = -\frac{\alpha_1^2+\alpha_2^2}{\alpha_2}(\nabla \overline{m}_h^{j-1/2}, \nabla w_h)\ . \tag{3.19}$$

Unfortunately, this latter equation is very difficult to solve because of the constraint on $m_h^j \in \mathcal{M}_h$. We therefore solve only approximately this equation and reconstruct m_h^j in order to satisfy the constraint. The governing idea is to account for the fact that due to the constraint on m_h^{j-1}, $d_t m_h^j$ almost belongs to $\mathcal{F}_h^j$. Therefore, if we replace this term by a new unknown $v_h \in \mathcal{F}_h^{j-1}$, we may approximate (3.19) by

$$\frac{\alpha_1}{\alpha_2}(v_h, w_h) - (m_h^{j-1} \times v_h, w_h) = -\frac{\alpha_1^2+\alpha_2^2}{\alpha_2}(\nabla \overline{m}_h^{j-1/2}, \nabla w_h) \quad \forall\, w_h \in \mathcal{F}_h^{j-1}\,. \tag{3.20}$$

Well-posedness of this problem follows from the fact that $v_h \in \mathcal{F}_h^{j-1}$ is determined by the difference of the continuous, positive symmetric bilinear form and a skew-symmetric continuous bilinear form. The algorithm in [4] now reads:

Algorithm 3.3. *1. Start with an initial magnetization $m_h^0 \in \mathcal{M}_h$.*
2. Given $m_h^{j-1} \in \mathcal{M}_h$, $1 \le j \le J$, solve (3.20) and call $v_h^{j-1} \in \mathcal{F}_h^{j-1}$ the solution.
3. Compute $m_h^j \in \mathcal{M}_h$ from

$$m_h^j(x) = \frac{m_h^{j-1}(x) + k v_h(x)}{|\, m_h^{j-1}(x) + k v_h(x)\,|} \quad \forall\, x \in \mathcal{E}\,.$$

A crucial step in the analysis of this discretization is to rewrite the second step in terms of $d_t m_h^j \in V_h(\omega; \mathbb{R}^n)$ and find the following characterization, for all $w_h \in \mathcal{F}_h^{j-1}$,

$$\Big|\frac{\alpha_1}{\alpha_2}(d_t m_h^j, w_h) - (m_h^{j-1} \times d_t m_h^j, w_h) + \frac{\alpha_1^2+\alpha_2^2}{\alpha_2}(\nabla \overline{m}_h^{j-1/2}, \nabla w_h)\Big| \le Ck\,\|\, w_h\,\|_{L^\infty}\,,$$

where C does not depend on j or k. Hence, this slightly perturbed version of (3.19) gives rise to the discrete energy inequality

$$\frac{\alpha_1}{\alpha_2} k \sum_{j=1}^{J} \| d_t m_h^j \|^2 + \frac{\alpha_1^2+\alpha_2^2}{\alpha^2} \max_{1\le j\le J} \| \nabla m_h^j \|^2 \le C t_J k + \frac{\alpha_1^2+\alpha_2^2}{\alpha^2} \| \nabla m_h^0 \|^2 .$$

This property eventually allows to extract a convergent subsequence $\{m_{h'}^{j'}\}$ whose limit — firstly taken with respect to $k \to 0$, then with respect to $h \to 0$ — is a weak solution of the equation in Gilbert form (3.7). This program of convergence analysis for the above method is elaborated in [4].

3.2.3. *Approximation of strong solutions to (LLG).* As outlined in the previous section, being provided with a consistent, discrete energy law to analytically hope for convergence of computed iterates towards weak solutions are non-trivial constraints for the construction of numerical methods to solve (LLG), and development in this direction is only very recent. Another direction of research over the last years are simple, easy-to-implement approximation schemes which perform remarkably well in practice: in general, they do not satisfy a discrete energy law and tend to independently deal with the nonconvex algebraic constraint, nonlocality, and the evolutionary character of the problem in order to obtain efficient numerical schemes: splitting-/projection schemes and penalization strategies.

In [39], a simple projection scheme is proposed to solve (LLG) which is implicit and unconditionally stable; flexibility with respect to the choice of the time-step size is an important issue for a method to numerically resolve magnetic multiscale phenomena, which rules out time-explicit methods as possible efficient schemes. On the other hand, fully implicit schemes have to cope with the nonconvex, strongly nonlinear character of the problem; these are the main motivations to come-up with the following scheme for (3.6).

Algorithm 3.4. *1. Start with an initial discretization $m_h^0 \in V_h(\omega;\mathbb{R}^n)$.*
2. Given $m_h^{j-1} \in \mathcal{M}_h$, $1 \le j \le J$, compute $\tilde{m}_h^j \in V_h(\omega;\mathbb{R}^n)$ for any $j \ge 1$ from

$$\frac{\alpha_1}{\alpha_1^2+\alpha_2^2}\left(\frac{\tilde{m}_h^j - m_h^{j-1}}{k}, \phi_h\right) + (\nabla \tilde{m}_h^j, \nabla \phi_h) - \frac{\alpha_2}{\alpha_1^2+\alpha_2^2}\left(m_h^{j-1} \times \frac{\tilde{m}_h^j - m_h^{j-1}}{k}, \phi_h\right) = 0 \quad \forall\, \phi_h \in V_h(\omega, \mathbb{R}^n) .$$

3. Compute $m_h^j \in \mathcal{M}_h$ from $m_h^j(x_\ell) = \frac{\tilde{m}_h^j(x_\ell)}{|\,\tilde{m}_h^j(x_\ell)\,|}$, for all $x_\ell \in \mathcal{E}$.

In order to handle efficiently nonlinear effects, the error analysis in [39] for the case of classical solutions to (LLG) is based on a characterization of the solution by a nonlinear recursion relation; for simplicity, for the heat flow of harmonic maps (i.e., $\alpha_1 = 1$, $\alpha_2 = 0$), we find

$$m_h^j(x_\ell) = \frac{(\mathrm{Id} - k\Delta_h)^{-1} m_h^{j-1}(x_\ell)}{|\,(\mathrm{Id} - k\Delta_h)^{-1} m_h^{j-1}(x_\ell)\,|} ,$$

where it is understood that the Neumann boundary condition is imposed when inverting the given operator. The authors in [39] now use Strang's trick to construct a correction of the exact solution of (LLG), for $\alpha_1 = 1$, $\alpha_2 = 0$,

$$m(x,t_j) = \frac{(\mathrm{Id} - k\Delta)^{-1} m(x,t_{j-1})}{|\,(\mathrm{Id} - k\Delta)^{-1} m(x,t_{j-1})\,|} + \mathcal{O}(k^2) , \tag{3.21}$$

which satisfies (3.21) to higher order accuracy. The same strategy is then used to also construct a second-order projection scheme, which is not obtained simply by keeping involved operators in Step 2. and considering averages in time, but requires some further correction terms: Step 2. is then replaced by

$$\begin{aligned} &\frac{\alpha_1}{\alpha_1^2+\alpha_2^2}\left(\frac{\tilde{m}_h^j - m_h^{j-1}}{k}, \phi_h\right) + (\nabla \overline{m}_h^{j-1/2}, \nabla \phi_h) - \frac{\alpha_2}{\alpha_1^2+\alpha_2^2}\left(m_h^{j-1} \times \frac{\tilde{m}_h^j - m_h^{j-1}}{k}, \phi_h\right) \\ &\quad = k^2\Big[\Big(\langle \nabla(|\,\nabla m_h^{j-1}\,|^2), \nabla m_h^{j-1}\rangle_{\mathbb{R}^3}\Big) + \frac{1}{2}\Big(|\,\nabla m_h^{j-1}\,|^2 [(\mathrm{Id} + m_h^{j-1}\times)^{-1} - \mathrm{Id}]\Delta_h m_h^{j-1}, \phi_h\Big)\Big] . \end{aligned}$$

Computational experiments are reported in [39] for the case of heat flow harmonic map to illustrate unconditional stability of these projection strategies, but also indicate an increase with respect to computational effort in the case of higher order projection methods.

A slightly modified numerical strategy is studied in [88] for (3.3)–(3.5), where the Lagrange multiplier of (LLG) is still kept in the discretization; the projection step then balances the damping character of the implicit Euler method, cf. Example 3.5.

Algorithm 3.5. *1. Start with an initial discretization* $m_h^0 \in V_h(\omega;\mathbb{R}^n)$.
2. Given $m_h^{j-1} \in \mathcal{M}_h$, *compute* $m_h^j \in V_h(\omega;\mathbb{R}^n)$ *for any* $1 \le j \le J$ *from*

$$(\frac{\tilde{m}_h^j - m_h^{j-1}}{k}, \phi_h) + \alpha_1 (\nabla \tilde{m}_h^j, \nabla \phi_h) = \alpha_1 \left(|\nabla \tilde{m}_h^{j-1}|^2 \tilde{m}_h^j, \phi_h \right) - \alpha_2 \left(\tilde{m}_h^j \times \nabla \tilde{m}_h^j, \nabla \phi_h \right) \quad \forall\, \phi_h \in V_h(\omega, \mathbb{R}^n)\,.$$

3. Compute $m_h^j \in \mathcal{M}_h$ *from* $m_h^j(x_\ell) = \frac{\tilde{m}_h^j(x_\ell)}{|\tilde{m}_h^j(x_\ell)|}$, *for all* $x_\ell \in \mathcal{E}$.

By replacing all quantities in Step 2. by tilted ones, we arrive at the following penalized discretized (LLG),

$$\begin{aligned} (d_t \tilde{m}_h^j, \phi_h) + \alpha_1 (\nabla \tilde{m}_h^j, \nabla \phi_h) + \frac{1}{\varepsilon} (\tilde{g}(\{\tilde{m}_h^j\}), \phi_h) \\ = \alpha_1 \left(|\nabla \tilde{m}_h^j|^2 \tilde{m}_h^j, \phi_h \right) - \alpha_2 \left(\tilde{m}_h^j \times \nabla \tilde{m}_h^j, \nabla \phi_h \right), \end{aligned} \tag{3.22}$$

where $\varepsilon = k$ and $\tilde{g}(\{\tilde{m}_h^j\}) = \left(1 - \frac{1}{|\tilde{m}_h^{j-1}|}\right) \tilde{m}_h^{j-1}$. Hence, the projection scheme above corresponds to a semi-explicit penalization with a new penalization function, which is additionally introduced to the discretization of (LLG) to enforce $|m_h^j(x_\ell)| = 1$, for all $x_\ell \in \mathcal{E}$. The following error estimates are verified in [88] for (3.22) in the case of quasi-uniform triangulations of $\omega \subset \mathbb{R}^2$ and related numerical scales $k^{-1/2} = o(h^{-1})$,

$$\begin{aligned} \max_{0 \le j \le J} \| m(t_j) - m_h^j \| + \Big(k \sum_{j=1}^{J} \| \nabla (m(t_j) - m_h^j) \|^2 \Big)^{1/2} \\ + \Big(\frac{k}{\varepsilon} \sum_{j=1}^{J} \Big[\| m(t_j) - m_h^j \|_{L^4}^4 + \| \langle m(t_j) - m_h^j, m(t_j) \rangle_{\mathbb{R}^3} \|^2 \Big] \Big)^{1/2} \le C(k+h)\,. \end{aligned} \tag{3.23}$$

The proof of this result uses an inductive argument to compensate for the lack of a discrete energy law, invoking (i) existence of (locally verifiable) strong solutions to (LLG), in combination with (ii) above approximation results and given restrictions on meshes and numerical scalings, in particular. These arguments and results have been extended to cases $\omega \subset \mathbb{R}^3$ in [27].

The connection between projection schemes and (semi-explicit) penalization ansatzes to numerically enforce the nonconvex constraint is the reason for the study of other strategies $\tilde{g} \equiv \tilde{g}_i$, $i = 1, 2, 3$,

$$\begin{gathered} \tilde{g}_1(\{\tilde{m}_h^j\}) = (|\tilde{m}_h^{j-1}|^2 - 1)\tilde{m}_h^j\,, \quad \tilde{g}_2(\{\tilde{m}_h^j\}) = \left(1 - \tfrac{1}{|\tilde{m}_h^{j-1}|}\right)\tilde{m}_h^{j-1}\,, \\ \tilde{g}_3(\{\tilde{m}_h^j\}) = \left(1 - \tfrac{1}{|\tilde{m}_h^{j-1}|^{2-\gamma}}\right)\tilde{m}_h^{j-1} \quad \gamma \in \mathbb{N}_0\,. \end{gathered}$$

Studies in [88] show that $\varepsilon^{-1} = o(k^{-1})$ is a stable choice for $\tilde{g}_1$, leading to optimal convergence behavior; computational experiments show suboptimal behavior in case $\varepsilon < k$ is chosen. Moreover, choosing $\gamma \in \mathbb{N}_0$ large yields a better balancing of stability and accuracy requirements, where the choice of ε is more flexible with respect to the time-step size k. These results evidence replacement of the projection method above by a 'scaled projection method', parameterized by $\gamma \in \mathbb{N}$; see Figure 7 (d).

Algorithm 3.6. *1. Start with an initial discretization* $m_h^0 \in V_h(\omega,\mathbb{R}^n)$.
2. Given $\tilde{m}_h^{j-1}, m_h^{j-1} \in V_h(\omega;\mathbb{R}^n)$, $1 \le j \le J$, *compute* $\tilde{m}_h^j \in V_h(\omega;\mathbb{R}^n)$ *from*

$$(\frac{\tilde{m}_h^j - m_h^j}{k}, \phi_h) + \alpha_1 (\nabla \tilde{m}_h^j, \nabla \phi_h) = \alpha_1 \left(|\nabla \tilde{m}_h^{j-1}|^2 \tilde{m}_h^j, \phi_h \right) - \alpha_2 \left(\tilde{m}_h^j \times \nabla \tilde{m}_h^j, \nabla \phi_h \right) \quad \forall\, \phi_h \in V_h(\omega, \mathbb{R}^n)\,.$$

3. Compute $m_h^j \in V_h(\omega;\mathbb{R}^n)$ *from* $m_h^j(x_\ell) = \frac{\tilde{m}_h^j(x_\ell)}{|\tilde{m}_h^j(x_\ell)|^{2-\gamma}}$, *for all* $x_\ell \in \mathcal{E}$.

So far, magnetostatic stray field, anisotropy and exterior magnetic fields which contribute in model (3.2), (1.4) were neglected, since they do not lead to further analytical problems in the general model; however,

an efficient numerical treatment of the general model is not so evident and is studied in [88], where different contributions

$$H^{j+1}_{\mathrm{eff},1;h} = \alpha \Delta_h m^{j+1}_h\,, \qquad H^{j}_{\mathrm{eff},2;h} = -D\varphi(m^j_h) - \nabla u^j_h + H^{j+1}$$

are shifted in time to eventually account for $H^{j+1}_{\mathrm{eff},h} = H^{j+1}_{\mathrm{eff},1;h} + H^{j}_{\mathrm{eff},2;h}$ in (LLG); computed iterates $(u^j_h, m^j_h) \in V_h(\Omega) \times V_h(\omega;\mathbb{R}^n)$ again satisfy (3.23).

Algorithm 3.7. *1. Start with (m^0_h, u^0_h), where $u^0_h = \Delta^{-1}_{\Omega,h}\mathrm{div}_h(\chi_\omega m^0_h)$.*
2. Given $(\tilde m^{j-1}_h, m^{j-1}_h, u^{j-1}_h) \in V_h(\omega,\mathbb{R}^n) \times V_h(\omega;\mathbb{R}^n) \times V^0_h(\Omega)$, $1 \le j \le J$, compute $\tilde m^j_h \in V_h(\omega,\mathbb{R}^n)$, with $\partial_n \tilde m^j_h = 0$ on $\partial\omega$, for any $j \ge 1$, and $\phi_h \in V_h(\omega,\mathbb{R}^n)$ from

$$\begin{aligned}\big(\frac{\tilde m^j_h - m^{j-1}_h}{k}, \phi_h\big) + \alpha_1\alpha\big(\nabla \tilde m^j_h, \nabla\phi_h\big) &= \alpha_1\alpha\big(|\nabla \tilde m^{j-1}_h|^2 \tilde m^j_h, \phi_h\big) + \alpha_2\big(\nabla(\phi_h \times \tilde m^{j-1}_h), \nabla \tilde m^j_h\big)\\ &+\alpha_2\big(m^{j-1}_h \times H^{j-1}_{\mathrm{eff},2;h}, \phi_h\big) - \alpha_1\big(m^{j-1}_h \times (m^{j-1}_h \times H^{j-1}_{\mathrm{eff},2;h}), \phi_h\big)\,.\end{aligned}$$

3. Given $\gamma \in \mathbb{N}_0$, compute $m^j_h \in V_h(\omega;\mathbb{R}^n)$ from $m^j_h(x_\ell) = \frac{\tilde m^j_h(x_\ell)}{|\tilde m^j_h(x_\ell)|^{2-\gamma}}$, for all $x_\ell \in \mathcal{E}$.
4. Given $\omega \Subset \Omega \subset \mathbb{R}^n$, compute $u^{j+1}_h \in V_h(\Omega)$ from

$$(\nabla u^{j+1}_h, \nabla w_h) = (m^{j+1}_h, \nabla w_h) \qquad \forall\, w_h \in V^0_h(\Omega)\,.$$

The following example is taken from [88].

Example 3.6. *Let $\omega = (-1,1)\times(-0.5,0.5)$, $H = (-100,0,0)$, $e = -\frac{1}{\sqrt{2}}(1,1,0)$, and fix parameters $\alpha_1 = \alpha_2 = \alpha = \beta = 1$, $\Omega = (-4,4)^2$ in (3.2), (1.4) to evolve*

$$m_0 = \frac{\hat m}{\sqrt{|\hat m|^2 + \eta^2}} \quad \text{in } \omega\,, \qquad \hat m(x,y) = (x^2 + y^2 - \frac{1}{4}, y, 0)\,,$$

for $\eta = 0.2$ according to Algorithm 3.7. Snapshots which show growing alignment of magnetization to applied field H are displayed in Figure 12.

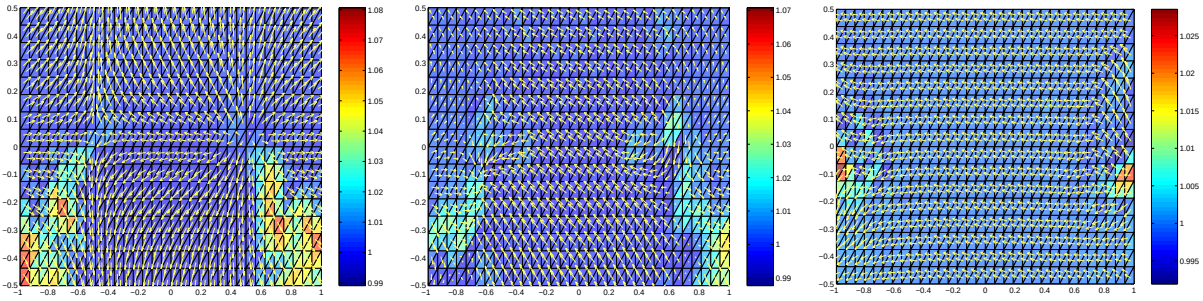

FIGURE 12. Plot of magnetization $\tilde m^j_h$ and its modulus at subsequent times, using Algorithm 3.7 (from [88])

3.2.4. *Effective dynamics of soft ferromagnetic thin films.* Dynamics of ferromagnetics is severely constrained in a thin film $\omega = \omega' \times (0,\delta) \subset \mathbb{R}^3$, leading to different behavior compared to bulk media. In [43], García-Cervera and E derived an effective dynamical equation for a soft ferromagnetic thin film in situations where $\alpha, \beta, |H_{\mathrm{ext}}| = \mathcal{O}(\delta)$, $\alpha_2 = 1$, and $\delta \ll \alpha_1$; moreover, to leading order it is plausible to ask for order parameters $m'(x') = (m'_1(x'), m'_2(x'))$, such that a.e. $|m'| = 1$. Then, by asymptotic analysis with respect to $\delta \to 0$, the spin dynamics for the limiting case is controlled by

$$m'_t = \big(\frac{1}{\alpha_1} + \alpha_1\big)\big(\tilde H_{\mathrm{eff}} - \langle m', \tilde H_{\mathrm{eff}}\rangle_{\mathbb{R}^2} m'\big)\,, \tag{3.24}$$

where $\tilde{H}_{\rm eff} = -D\mathcal{E}_{\rm thin}$ is now computed from

$$\mathcal{E}_{\rm thin}(m') = \alpha \int_\omega |\nabla m'|^2 \,{\rm d}x' + \int_\omega \varphi(m')\,{\rm d}x' - \int_\omega \langle H, m'\rangle_{\mathbb{R}^2}\,{\rm d}x' + \frac{1}{4}\,\|\,{\rm div}'\, m'\,\|^2_{H^{-1/2}(\Omega')}\,, \qquad \omega' \Subset \Omega' \subseteq \mathbb{R}^2\,.$$

Computational comparisons of (3.24) with the full Landau-Lifshitz-Gilbert equation show very good agreement in the regime $\delta \le \alpha_1$ ($\alpha_2 = 1$), cf. [43]; note that (3.24) for $\tilde{H}_{\rm eff} = \alpha\Delta m$ yields to heat flow of harmonic maps.

At first glance, it is surprising that the gyromagnetic term of (LLG) in the thin film limit only contributes as damping term for the in-plane components of m, moreover with a much larger damping coefficient $\frac{1}{\alpha_1}$. The reason for this is the requirement $\delta \ll \alpha_1$ that exchange mechanisms dominate all other geometric and physical parameters; unfortunately, this crucial constraint excludes reliable studies of dynamics, e.g. vortex dynamics, by using the reduced model (3.24) for practically relevant studies; cf. [40].

3.3. **A mesoscopic-level model.** For mesoscale ferromagnets, the main interest lies in evolution of averaged magnetizations rather than detailed, complex spin dynamics. The phenomenological model introduced by Roubíček and Kružík in [90, 91] combines the tendency to minimize Landau-Lifshitz energy during evolution with a rate-independent maximum-dissipation mechanism during magnetization switching from one pole to the other. In fact, there are many contributions to energetic losses if a ferromagnet is exposed to a switching external magnetic field. Besides hysteresis losses which are independent of an external field frequency and which we are going to model here, there are also intrinsic damping, disaccommodation and eddy currents. Except for hysteresis losses, all others are rate-dependent; we refer to [51] for more details. In this sense, hysteresis losses are considered as a limit for frequencies tending to zero. On the other hand, for ferromagnets, rate-independence holds with a good approximation in a fairly wide range of frequencies.

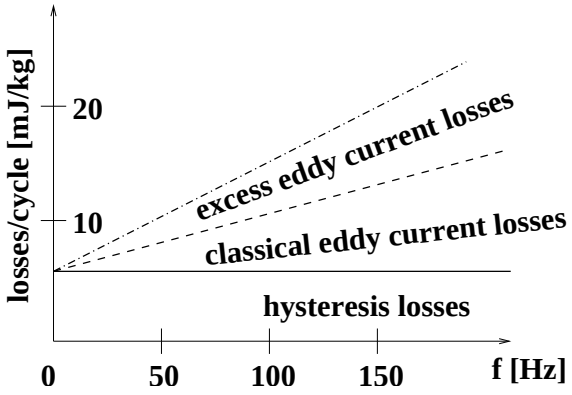

FIGURE 13. Frequency dependence of different kinds of losses in a transformer steel [51].

3.3.1. *Rate-independent dissipation.* For usual loading regimes and magnetically hard materials, one must consider a certain dissipation mechanism, which may also be influenced by impurities in the material without affecting substantially the stored energy. Hence, energy storage and dissipation mechanisms are, to some extent, independent of each other and, as the dissipation mechanisms are determined on an atomistic level, it seems that the only efficient way how to incorporate them in a higher-level model is a phenomenological approach.

Our, to some extent simplified, standpoint is that the amount of dissipated energy within the phase transformation from one pole to the other can be described by a single, phenomenologically given number (of the dimension J/m^3=Pa) depending on the coercive force $H_{\rm c}$ [23]. Hence, we need to identify the particular poles according to the magnetization vector. Inspired by [75, 77] and considering L poles ($L = 2$ for uniaxial magnets or 6 or 8 for cubic magnets), we define a continuous mapping $\mathfrak{L} : S^{n-1} \to \triangle_L$ where $\triangle_L := \{\xi \in \mathbb{R}^L;\ \xi_i \ge 0,\ i = 1, ..., L,\ \sum_{i=1}^L \xi_i = 1\}$. In other words, $\{\mathfrak{L}_1, ..., \mathfrak{L}_L\}$ forms a partition of unity on S^{n-1} such that $\mathfrak{L}_i(s)$ is equal to 1, if s is in i-th pole, i.e., $s \in S^{n-1}$ is in a neighborhood of i-th

easy-magnetization direction. Of course, $\mathfrak{L}(m)$ in the (relative) interior of $\triangle_L$ indicates m in the region where no definite pole is specified. Hence, $\mathfrak{L}$ plays the role of an order parameter.

In terms of the mesoscopic microstructure described by the Young measure ν, the "mesoscopic" order parameter is naturally defined as

$$\varsigma = \Lambda\nu := \mathfrak{L} \bullet \nu$$

where $[\mathfrak{L} \bullet \nu](x) := \int_{S^{n-1}} \mathfrak{L}(s)\nu_x(\mathrm{d}s)$. Thus, Λ is just a continuous extension of the mapping $m \mapsto \mathfrak{L}(m)$, i.e., if $\{m_k\}$ converges to ν weakly* in $L^\infty(\omega;\mathbb{R}^n)$, then $\mathfrak{L}(m_k) \rightharpoonup \Lambda\nu$ weakly* in $L^\infty(\omega;\mathbb{R}^L)$.

In order to phenomenologically describe dissipative energetics, one must prescribe a potential of dissipative forces as a function of the rate of ς. For rate-independent processes, this potential must be convex and homogeneous of degree one. Considering a norm $|\cdot|_{\mathbb{R}^L}$ on $\mathbb{R}^L$, one can postulate $\varrho(\dot\varsigma) = H_c|\dot\varsigma|_{\mathbb{R}^L}$. The energy density needed to transform i-th pole to j-th pole is then $H_c|e_i - e_j|_{\mathbb{R}^L}$, with e_i the unit vector with 1 at the i-th position.

In the sequel, we represent magnetization at time $t \geq 0$ by the couple $q = q(t) \equiv (\,\nu, \varsigma\,) = (\,\{\nu_{x,t}\}_{x\in\omega}, \varsigma(\cdot,t)\,)$. Let us denote by $\mathcal{Q}$ the convex set of admissible configurations:

$$\mathcal{Q} := \Big\{ q = (\,\nu,\varsigma\,) \in L^\infty_{\mathrm{w}}\big(\omega;\mathcal{M}(S^{n-1})\big) \times L^\infty(\omega,\mathbb{R}^L) \,\big|\, \varsigma(x) \in \triangle_L\,,\ \Lambda\nu = \varsigma \text{ for a.a. } x \in \omega \Big\}. \tag{3.25}$$

Let $\mathcal{G}(t,q) := \overline{\mathcal{E}}_0(q) - \langle F(t), q\rangle$ denote Gibbs energy, where $\langle F(t),q\rangle = \langle \nu, H(t)\otimes \mathrm{Id}\rangle$, and $\mathcal{D}(q_1,q_2) := H_c \int_\omega |\,\varsigma_1 - \varsigma_2\,|_{\mathbb{R}^L}\,\mathrm{d}x$ the distance between to configurations $q_i = (\,\nu_i,\varsigma_i\,)$, $i = 1,2$. The general framework of Mielke, Theil, and Levitas [75, 76, 77] is used in the sequel to obtain a mesoscopic ferromagnetic model with appropriate solvability properties.

Definition 3.2. *A process $q = q(t)$ is called stable if for all $t \in [0,T]$*

$$\mathcal{G}(t,q) \leq \mathcal{G}(t,\tilde q) + \mathcal{D}\big(q(t),\tilde q\big) \quad \forall\, \tilde q \in \mathcal{Q}\,.$$

An important notion is the set of stable states $S(t)$ at a time $t \geq 0$,

$$S(t) = \Big\{ q \in \mathcal{Q} \,\Big|\, \mathcal{G}(t,q) \leq \mathcal{G}(t,\tilde q) + \mathcal{D}(q,\tilde q) \quad \forall\, \tilde q \in \mathcal{Q} \Big\}$$

Definition 3.3. *A process $q = q(t)$ satisfies the energy inequality if for a.a. $s,t \in [0,T]$, s.t. $s \leq t$,*

$$\underbrace{\mathcal{G}\big(t,q(t)\big)}_{\substack{\text{effective Gibbs'}\\ \text{energy at time } t}} + \underbrace{\mathrm{Var}(\mathcal{D},q;s,t)}_{\substack{\text{dissipated}\\ \text{energy}}} \leq \underbrace{\mathcal{G}\big(s,q(s)\big)}_{\substack{\text{Gibbs' ener-}\\ \text{gy at time } s}} - \underbrace{\int_s^t \left\langle \frac{\mathrm{d}F}{\mathrm{d}t}(\theta), q(\theta)\right\rangle \mathrm{d}\theta}_{\substack{\text{reduced work of}\\ \text{external field}}}$$

where the total variation over the time interval $[s,t]$ is defined in a standard way, without using explicitly any time derivative, as $\mathrm{Var}(\mathcal{D},q;s,t) := \sup \sum_{j=1}^J \mathcal{D}\big(q(t_{j-1}),q(t_j)\big)$, where the supremum is taken over all $J \in \mathbb{N}$ and over all partitions of $[s,t]$ in the form $s = t_0 < t_1 < \ldots < t_{J-1} < t_J = t$.

It was shown in [76] that in qualified cases the stability and energy inequality can be written in the form of a doubly nonlinear evolutionary inclusion

$$\partial R(q_t) + D\overline{\mathcal{E}_0}(q) + N_{\mathcal{Q}}(q) \ni F(t)\,, \quad q(0) = q_0\,, \tag{3.26}$$

where $q_0 = (\,\nu_0, u_0\,) \in \mathcal{Q}$ denotes the initial configuration, $N_{\mathcal{Q}}$ the normal cone to $\mathcal{Q}$ at q, and ∂R the subdifferential of the energy $R(q) = \int_\omega \varrho(\varsigma)\,\mathrm{d}x = \int_\omega H_c|\varsigma|_{\mathbb{R}^L}\,\mathrm{d}x$, which is dissipated during the transformation process. The advantage of defining a solution of (3.26) is the absence of any time derivative and purely energetic considerations. In this sense, it can be seen as a weak form of (3.26).

Definition 3.4. *The process $q = q(t)$, $q \equiv (\,\nu,\varsigma\,)$, will be considered a solution if $\nu \in L^\infty_{\mathrm{w}}\big(\omega_T;\mathcal{M}(S^{n-1})\big)$, $\varsigma \in BV\big([0,T];L^1(\omega;\mathbb{R}^L)\big)$, and $q(t) \in \mathcal{Q}$ for all $t \in [0,T]$, and is stable for all $t \in [0,T]$ and satisfies the energy inequality in Definition 3.3, for a.a. $s,t \in [0,T]$, such that $s \leq t$.*

The existence of a solution satisfying this definition was shown in [90]. The Gibb's energy needs a slight regularization by a higher order term, however.

Remark 3.3. *By the reduced work in Definition 3.3 we mean (up to a sign) the usual work, i.e.* $\int_s^t \langle F, \frac{\mathrm{d}q}{\mathrm{d}t}\rangle \,\mathrm{d}\theta$, *but reduced by* $\langle F(s), q(s)\rangle - \langle F(t), q(t)\rangle$ *which is just the gap between Gibbs' and Helmholtz' energies at time instances* 0 *and* t.

3.3.2. *Incremental problems.* The existence of a response $t \mapsto q(t)$ with the above mentioned properties was shown even in a more general case in [91] by a semi-discretization in time, using the implicit Euler scheme. For simplicity, let us consider an equi-distant partition of the time interval $[0, T]$ with a time step $k > 0$, assuming T/k an integer.

Algorithm 3.8. *Let* $q^0 = q_0$, *find* $q^j := \mathrm{argmin}_{q\in\mathcal{Q}} I(q)$, *for* $j = 1, .., \frac{T}{k}$ *and*

$$I(q) := \mathcal{G}(jk, q) + \mathcal{D}(q^{j-1}, q)\,.$$

If a global minimizer to this problem is not unique, we just identify an arbitrary one as q^j. Then we define the piecewise constant interpolation $q \in L^\infty\big(0,T; L^\infty_{\mathrm{w}}(\omega; \mathcal{M}(S))\big) \times L^\infty\big(\omega; \mathbb{R}^L\big)$ in the way $q\big|_{((j-1)k,jk]} = q^j$ for $j = 1, ..., T/k$, and $q_k(0) = q^0$. A proof of the existence of a solution to the evolutionary problem can be found in [91]. It is based on the above incremental formulation and on a suitable limiting procedure.

3.3.3. *Numerical solution.* A straightforward numerical approximation based on the incremental formulation in Algorithm 3.8 copes with the nonsmoothness of the dissipative term. However, in specific cases, using an approach from [60, 90], we can reformulate the problem as a smooth one with a few additional constraints and variables. One such situation is e.g. if $L = 2$, $|b|_L = 2\max(|b_1|, |b_2|)$ for any $b \in \mathbb{R}^2$. Then $\varsigma(x) = \int_{S^{n-1}} s_3\, \nu_x(\mathrm{d}s)$ where $s = (\,s_1, s_2, s_3\,)$, or $\varsigma = m_3$, i.e., the third component of the magnetization. The stray field energy is calculated using Green's function of the Laplace operator as described in [72, 71].

Algorithm 3.9. *Given* $q^0 = q(0)$, *compute* $(\,q^j, a^j\,) = \mathrm{argmin}_{\mathcal{Q}\times L^1(\omega)} J(q, a)$, *where*

$$J(q, a) := \mathcal{G}(jk, q) + \int_\omega a(x)\,\mathrm{d}x \tag{3.27}$$

and

$$\begin{cases} \int_{S^{n-1}} s_3 \nu_x^{k-1}(\mathrm{d}s) - \int_{S^{n-1}} s_3 \nu_x(\mathrm{d}s) \le a(x) \text{ for a.a. } x \in \omega\,, \\ \int_{S^{n-1}} s_3 \nu_x(\mathrm{d}s) - \int_{S^{n-1}} s_3 \nu_x^{k-1}(\mathrm{d}s) \le a(x) \text{ for a.a. } x \in \omega\,. \end{cases}$$

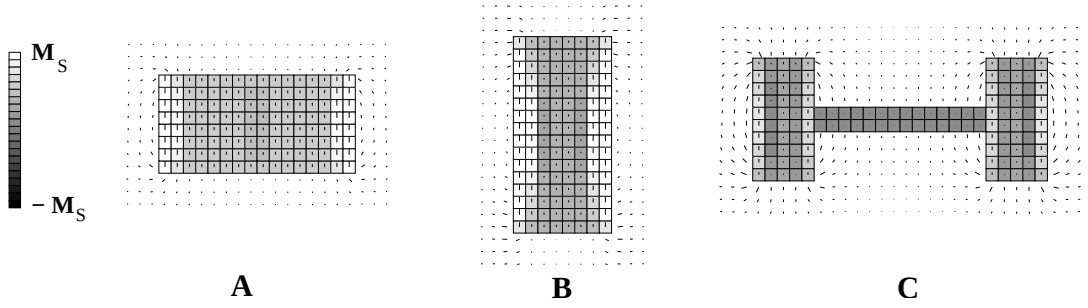

FIGURE 14. Magnetization m_h for 2D-cross sections of various bulk specimens computed from Algorithm 3.9 (also the demagnetizing field around), displayed at specific times (after [66])

It can be shown, see [60], that Algorithms 3.8 and 3.9 are equivalent to each other in the sense that having a solution to anyone of them we can easily construct a solution to the other one. Algorithm 3.9 can be discretized in the same way as (2.4). Figures 14–15 display the magnetization, the stray field around, and the resulting hysteresis loops for a uniaxial material CoZrDy at the temperature 4.2 K, using Algorithm 3.9. In case that the mesoscopic order parameter ς is an affine function of the magnetization then one can rule out the Young measure from Definition 3.3. The resulting incremental problem is then formulated only in terms of the magnetization; one has to replace the anisotropy density φ by φ^{**}, however, and ends up having

$$\partial R^{**}(m_t) + D\tilde{\mathcal{E}}_0(m) + N_{\tilde{\mathcal{A}}}(M) \ni 0\,, \qquad m(0) = 0\,,$$

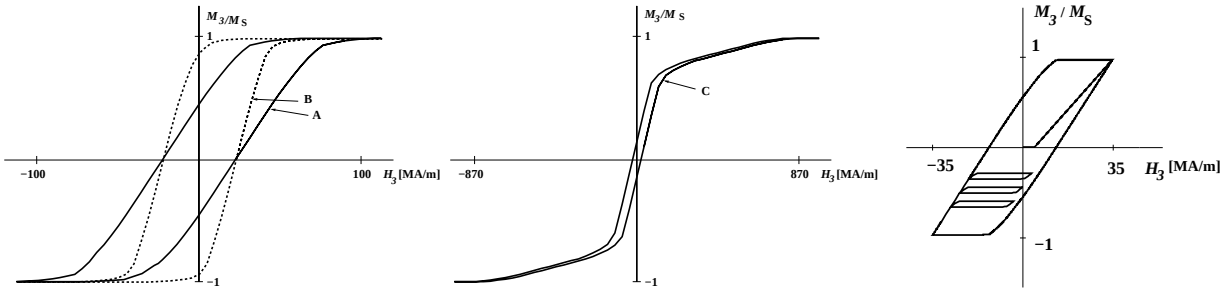

FIGURE 15. Hysteresis loops corresponding to specimen A, B, C in Figure 14 (left, middle); Virgin magnetization and minor hysteresis loops due to spatially varying activation threshold resulted by inhomogeneities of magnetization process (after [66, 67])

where $R^{**}(m_t) := \int_\omega |\varsigma(m_t)| \, \mathrm{d}x$, cf. (2.3)-(2.4). A discretization of this problem (in regularized form, $\gamma > 0$) using implicit Euler method on an equidistant mesh $I_k = \{t_j\}_j$ leads to a convex problem at every time-step (compare to Problem 2.1):

Algorithm 3.10. *1. Start with* $m_h^0 = P_h m^0 \in W_h(\omega; \mathbb{R}^2)$, *and fix* $k, h, \gamma > 0$.
2. For each $1 \le j \le J$, *find* $(m_h^j, u_h^j) \in W_h(\omega; \mathbb{R}^2) \times \tilde{V}_h^0(\Omega)$ *that satisfies*

$$(\nabla_h u_h^j, \nabla_h w_h) = (m_h^j, \nabla_h w_h) \quad \forall\, w_h \in \tilde{V}_h^0(\Omega)\,,$$

$$\nabla_h u_h^j + D\varphi^{**}(m_h^j) + \mathrm{sgn}_\gamma\Big(\varsigma(m_h^j) - \varsigma(m_h^{j-1})\Big) D\varsigma(m_h^j) + \varsigma_h^j m_h^j = P_h H^j \qquad \text{a.e. in } \omega\,,$$

$$\varsigma_h^j = \varepsilon^{-1} \frac{(|\, m_h^j \,| - 1)_+}{|\, m_h^j \,|} \qquad \text{a.e. in } \omega\,.$$

This algorithm has been studied in [65], which motivates $\gamma = \mathcal{O}(h^2)$, in particular; cf. Figure 16.

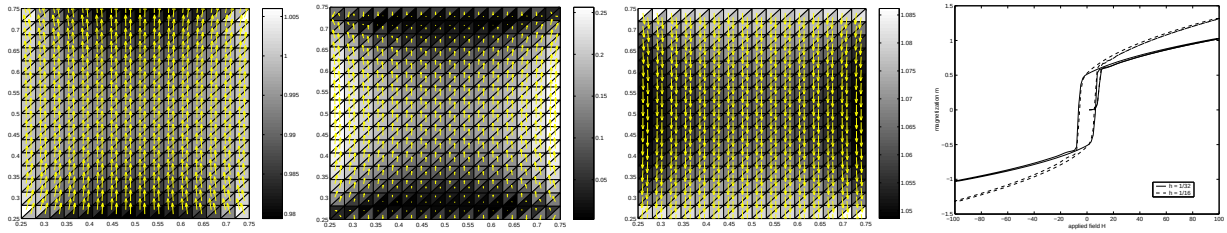

FIGURE 16. Magnetization $\{m_h^j\}_j$ computed from Algorithm 3.10 close to first switching time at three subsequent time steps, and corresponding hysteresis loop (from [65])

Remark 3.4. *The mesoscopic model described above does not allow for modeling a virgin magnetization curve, i.e., the curve describing the evolution of the magnetization from a completely demagnetized specimen (i.e.* $|m| = 0$ *in* ω*) to the saturation state (*$|m| = 1$ *in* ω*). The reason is that the coercive force* H_c *is kept constant. One way how to generalize the model in a way that it describes virgin magnetization processes is to make the coercive force dependent on the history of the magnetization. This idea was scrutinized in* [67, 91].

4. OUTLOOK

The mathematical modeling of ferromagnetic materials is a very active area of research for decades, and many important questions raised e.g. in [33, 40] have only been answered recently. However, many interesting questions are still open, including effective dynamics for walls, vortices, as well as their interaction, or reduced, effective models which are valid for different relevant parameter regimes, blow-up behavior of (LL) and (LLG),

and efficient numerical strategies to reliably handle nonconvexity and nonlocal constraints imposed to weak solutions — to only name a few interesting topics. The following list is mainly motivated by own interests of the authors:

- Understanding the relationship between the original Landau-Lifshitz energy and a newly derived finite temperature version of the micromagnetic energy derived in [55, 56]. Is it computationally feasible to model various domain walls by the stochastic model?
- Develop a microscopic model describing dissipation effects in a physically more reliable way, which could also be used to rigorously derive mesoscopic evolutionary limiting problems.
- Study of more complex electromagnetic models describing e.g. reading and writing of information on a hard disk [94] all, from modeling, analytical, and numerical view point.
- Clarify the relationship between mesoscopic evolutionary models and Preisach models used in hysteresis computation for many decades. Does the energetic formulation correspond to a Preisach operator? As a starting point one can study whether the energetic formulation allows for the so-called return-point property. See [98] for details.
- Setting valuable benchmarks for the hysteresis calculations and testing mesoscopic models for engineering problems.

Acknowledgment. The paper was partly written during M. K.'s stay at the ETH Zurich in May 2004, and A. P.'s stay at 'UTIA AV ČR in Prague in September 2004. The hospitality of the hosting institutes is gratefully acknowledged. The work of M.K. was also supported by the GA AV ČR grant No. IAA 1075402.

References

[1] A. Aharoni, *Introduction to the theory of ferromagnetism*, Oxford University Press (1996).
[2] F. Alouges, *A new algorithm for computing liquid crystal stable configurations: the harmonic mapping case*, SIAM J. Num. Anal. **34**, pp. 1708–1726 (1997).
[3] F. Alouges, S. Conti, A. DeSimone, Y. Pokern, *Energetics and switching of quasi-uniform states in small ferromagnetic particles*, M2AN Math. Model. Numer. Anal. **38**, pp. 235–248 (2004).
[4] F. Alouges, P. Jaisson, *Convergence of a finite element discretization for the Landau-Lifshitz equations*, preprint (2004).
[5] F. Alouges, A. Soyeur, *On global weak solutions for Landau-Lifshitz equations: existence and nonuniqueness*, Nonl. Analysis, Theory, Meth. Appl. **18**, pp. 1071–1084 (1992).
[6] F. Alouges, T. Rivière, S. Serfaty, *Néel and cross-tie wall energies for planar micromagnetic configurations*, ESAIM Control Optim. Calc. Var. **8**, pp. 31–68 (2002).
[7] G. Anzellotti, S. Baldo, A. Visintin, *Asymptotic behavior of the Landau-Lifshitz model of ferromagnetism*, Appl. Math. Optim. **23**, pp. 171–192 (1991).
[8] S. Bartels, *Stability and convergence of finite element approximation schemes for harmonic maps*, preprint (2004).
[9] S. Bartels, J. Ko, A. Prohl, *Numerical study of blow-up for Landau-Lifshitz equation* (in preparation).
[10] A. Bergqvist, *Magnetic vector hysteresis model with dry friction-like pinning*, Physica B **233**, pp. 342–347 (1997).
[11] H.A.M. van den Berg, *Self-consistent domain theory in soft ferromagnetic media. II. Basic domain structures in thin film objects*, J. Appl. Phys. **60**, pp. 1104–1113 (1986).
[12] M. Bertsch, P. Podio-Guidugli, V. Valente, *On the dynamics of deformable ferromagnets. I. Global weak solutions for soft ferromagnets at rest*, to appear in: Ann. Mat. Pura Appl. **179**, pp. 331–360 (2001).
[13] M. Brokate, J. Sprekels, *Hysteresis and Phase Transitions*, Springer, New York, 1996.
[14] P. Bryant, H. Suhl, *Thin-film magnetic patterns in an external field*, Appl. Phys. Lett. **54**, pp. 2224–2226 (1989).
[15] W.F. Brown, *Magnetostatic principles in ferromagnetism*, Springer, New York (1966).
[16] C. Carstensen, S.A. Funken, A. Prohl, *Stable finite elements in relaxed micromagnetic problems*, in: 16th IMACS World Congress (2000).
[17] C. Carstensen, D. Praetorius, *Numerical Analysis for a Macroscopic Model in Micromagnetics*, SIAM J. Numer. Anal. (in print).
[18] C. Carstensen, A. Prohl, *Numerical analysis of relaxed micromagnetics by penalised finite elements*, *Num. Math.* **90**, pp. 65–99 (2001).
[19] C. Carstensen, T. Roubíček, *Numerical approximation of Young measures in non-convex variational problems*, Num. Math. **84**, pp. 395–415 (2000).
[20] M.M. Cerimele, F. Pistella, V. Valente, *A numerical study of a nonlinear system arising in modeling of ferromagnets*, Nonl. Analysis **47**, pp. 3357–3367 (2001).
[21] N.H. Chang, J. Shatah, K. Uhlenbeck, *Schrödinger maps*, Comm. Pure Appl. Math. **53**, pp. 590–602 (2000).
[22] Y. Chen, S. Ding, B. Guo, *Partial regularity for two-dimensional Landau-Lifshitz equations*, Acta Math. Sinica **14**, pp. 423–432 (1998).
[23] S. Chikazumi, *Physics of Magnetism*, J.Wiley, New York (1964).

[24] R. Choksi, R.V. Kohn, *Bounds on the micromagnetic energy of a uniaxial ferromagnet*, Comm. Pure Appl Math. **51**, pp. 259–289 (1999).
[25] R. Choksi, R.V. Kohn, F. Otto, *Domain branching in uniaxial ferromagnets: a scaling law for the minimum energy*, Commun. Math. Phys. **201**, pp. 61–79 (1999).
[26] J. Cimrák, M. Slodička, *An iterative approximation scheme for the Landau-Lifshitz-Gilbert equation*, J. Comp. Appl. Math. **169**, pp. 17–32 (2004).
[27] J. Cimrák, *Error estimates for a semi-implicit numerical scheme solving the Landau-Lifshitz equation with an exchange field*, preprint, (2004).
[28] R. Cohen, R. Hardt, D. Kinderlehrer, S.-Y. Lin, M. Luskin, *Minimum energy configurations for liquid crystals: computational results*, in: Theory and applications of liquid crystals, IMA **5**, New York (Springer), pp. 99–122 (1987).
[29] R. Cohen, S.-Y. Lin, M. Luskin, *Relaxation and gradient methods for molecular orientation in liquid crystals*, Comput. Phys. Comm. **53**, pp. 455-465 (1989).
[30] J. Coron, *Nonuniqueness for the heat flow of harmonic maps*, Ann. Inst. H. Poincaré, Non-Linéaire **7**, pp. 335–344 (1990).
[31] E. Dean, R. Glowinski, C.H. Li, *Applications of operator splitting methods to the numerical solution of nonlinear problems in continuum mechanics and physics*, in: Mathematics applied to science (Academic Press), New York, pp. 13–64 (1988).
[32] A. DeSimone, *Energy minimizers for large ferromagnetic bodies*, Arch. Rat. Mech. Anal. **125**, pp. 99–143 (1993).
[33] A. DeSimone, R.V. Kohn, S. Müller, F. Otto, *Magnetic microstructures—a paradigm of multiscale problems*, ICIAM 99 (Edinburgh), pp. 175–190, Oxford Univ. Press, Oxford (2000).
[34] A. DeSimone, R.V. Kohn, S. Müller, F. Otto, *A reduced theory for thin-film micromagnetics*, Comm. Pure Appl. Math. **55**, pp. 1408–1460 (2002).
[35] A. DeSimone, R.V. Kohn, S. Müller, F. Otto, *Repulsive interaction of Néel walls, and the internal length scale of the cross-tie walls*, Multiscale Model. Simul. **1**, pp. 57–104 (2003).
[36] A. DeSimone, R.V. Kohn, S. Müller, F. Otto, R. Schäfer, *Two-dimensional modeling of soft ferromagnetic films*, R. Soc. Lond. Proc. Ser. A Math. Phys. Eng. Sci. **457**, pp. 2983–2991 (2001).
[37] A. DeSimone, H. Knüpfer, F. Otto, *2-d stability of the Néel wall*, preprint (2004).
[38] S. Ding, B. Guo, *Initial-boundary value problem for higher-dimensional Landau-Lifshitz systems*, Appl. Anal. **83**, pp. 673–697 (2003).
[39] W. E, X.-P. Wang, *Numerical methods for the Landau-Lifshitz equation*, SIAM J. Numer. Analysis **38**, pp. 1647–1665 (2000).
[40] W. E, *Selected problems in material science*, in: World mathematics 2000, Springer (2000).
[41] X. Feng, A. Prohl, *Numerical analysis of the Allen-Cahn equation and approximation for mean curvature flows*, Numer. Math. **94**, pp. 33–65 (2003).
[42] J. Fidler, T. Schrefl, *Micromagnetic modelling – the current state of the art*, J. Phys. D: Appl. Phys. **33**, R135–R156 (2000).
[43] C.J. García-Cervera, W. E, *Effective dynamics for ferromagnetic thin films J. Appl. Phys.* **90** 370-374 (2001).
[44] T.L. Gilbert, *A Lagrangian formulation of gyromagnetic equation of the magnetization field*, Phys. Rev. **100**, pp. 1243ff (1955).
[45] B. Guo, M.-C. Hong, *The Landau-Lifshitz equation of the ferromagnetic spin chain and harmonic maps*, Calc. Var. **1**, pp. 311–334 (1993).
[46] B. Guo, F. Su, *Global weak solution for the Landau-Lifshitz-Maxwell equation in three space dimensions*, J. Math. Anal. Appl. **211**, pp. 326–346 (1997).
[47] B. Guo, F. Su, *The global smooth solution for Landau-Lifshitz-Maxwell equation without dissipation*, J. Partial Diff. Eqs. **11**, pp. 193–208 (1998).
[48] B. Guo, Y. Han, G. Yang, *Blow-up for Landau-Lifshitz equations in two dimensions*, Comm. Nonl. Science & Num. Sim. **5**, pp. 43–44 (2000).
[49] S. Gustafson, J. Shatah, *The stability of localized solutions of Landau-Lifshitz equations*, Comm. Pure Appl. Math. **55**, pp. 1136–1159 (2002).
[50] P. Harpes, *Uniqueness and bubbling of the 2-dimensional Landau-Lifshitz flow*, Calc. Var. **20**, pp. 213–229 (2004).
[51] A. Hubert, R. Schäfer, *Magnetic Domains*, Springer, Berlin (1998).
[52] R.D. James, D. Kinderlehrer, *Frustration in ferromagnetic materials*, Continuum Mech. Thermodyn. **2** pp. 215–239 (1990).
[53] P. Joly, A. Komech, O. Vacus, *On transitions to stationary states in a Maxwell-Landau-Lifshitz-Gilbert system*, SIAM Math. Anal. **31**, pp. 346–374 (2000).
[54] P. Joly, O. Vacus, *Mathematical and numerical studies of nonlinear ferromagnetic materials*, Math. Mod. Num. Anal. **33**, pp. 593–626 (1999).
[55] M.A. Katsoulakis, P. Plecháč, *Statistical equilibrium measures in micromagnetics*, preprint (2004).
[56] M.A. Katsoulakis, P. Plecháč, D.K. Tsagkarogiannis, *Mesoscopic modeling for continuous spin lattice systems: Model problems and micromagnetics applications*, preprint (2004).
[57] C.E. Kenig, G. Ponce, L. Vega, *Small solutions to nonlinear Schrödinger equations*, Ann. Inst. H. Poincaré Anal. Non Linéaire **10**, pp. 255–288 (1993).
[58] J. Ko, *Partially Regular and Singular Solutions to the Landau-Lifshitz (Gilbert) Equations*, Ph.D.-thesis, New York University (2004).
[59] T.R. Koehler, *Hybrid FEM-BEM method for fast micromagnetic calculations*, Physica B **233**, pp. 302–307 (1997).

[60] M. Kružík, *Maximum principle based algorithm for hysteresis in micromagnetics*, Adv. Math. Sci. Appl. **13**, pp. 461–485 (2003).
[61] M. Kružík, Variational models for microstructure in shape memory alloys and in micromagnetics and their numerical treatment. In: *Communications of the Bexbach Colloquium on Science 2000, vol. II.* Proceedings of the conference held in Bexbach, Germany, October 27–29, 2000 (Eds. M. Robnik and A. Ruffing), Shaker Verlag, Aachen, 2003, pp. 20–38.
[62] M. Kružík, *Periodic solution to a hysteresis model in micromagnetics*, IMA Preprint **1446**, U Minnesota (2003).
[63] M. Kružík, *Periodicity properties of solutions to a hysteresis model in micromagnetics*, In: Num. Math. Adv. Appl., Proceedings of ENUMATH 2003, (M. Feistauer et al. eds.) , Springer, Berlin, pp. 605–614 (2004).
[64] M. Kružík, A. Prohl, *Young measure approximation in micromagnetics*, Num. Math. **90**, pp. 291–307 (2001).
[65] M. Kružík, A. Prohl, *Macroscopic modeling of magnetic hysteresis*, *Adv. Math. Sci. Appl.* (in print).
[66] M. Kružík, T. Roubíček, *Specimen shape influence on hysteretic response of bulk ferromagnets*, J. Magn. Magn. Mat. **256**, 158–167 (2003).
[67] M. Kružík, T. Roubíček, *Interactions between demagnetizing field and minor-loop development in bulk ferromagnets* J. Magn. Magn. Mat. **277**, 192–200 (2004).
[68] L.D. Landau, E.M. Lifshitz, *On the theory of the dispersion of magnetic permeability of ferromagnetic bodies*, Physik Z. Sowj. **8**, pp. 153–169 (1935). *Course of Theoretical Physics* **8**, Pergamon Press, Oxford (1960).
[69] S.-Y. Lin, M. Luskin, *Relaxation methods for liquid crystal problems*, SIAM J. Num. Anal. **26**, pp. 1310–1326 (1989).
[70] X. Liu, S. Jiang, Y. Han, *New explicit solutions to the n-dimensional Landau-Lifshitz equations*, pp. 324–326, Physics Letters **A 281** (2001).
[71] M. Luskin, L. Ma, *Analysis of the finite element approximation of microstructure in micromagnetics*, SIAM J. Num. Anal. **29**, pp. 320–331 (1992).
[72] L. Ma, *Analysis and computation for a variational problem in micromagnetics*, Ph.D.-thesis, U Minnesota (1991).
[73] C. Melcher, *The logarithmic tail of Néel walls in thin films*, Arch. Rat. Mech. Anal. **168**, pp. 83–113 (2003).
[74] A. Mielke, *Energetic formulation of multiplicative elastoplasticity using dissipation distances*, Cont. Mech. Thermodyn. (to appear).
[75] A. Mielke, F. Theil, *Mathematical model for rate-independent phase transformations*, in: Models of Cont. Mechanics in Analysis and Engineering, Shaker-Verlag, Aachen, pp. 117–129 (2001).
[76] A. Mielke, F. Theil, *On rate-independent hysteresis models*, Nonlin. Diff. Eq. Appl. **11** (2004), 151-189.
[77] A. Mielke, F. Theil, V. Levitas, *A variational formulation of rate-independent phase transformations using extremum principle*, Arch. Rat. Mech. Anal. **162**, pp. 137–177 (2002).
[78] P.M. Monk, O. Vacus, *Error estimates for a numerical scheme for ferromagnetic problems*, SINUM **36**, pp. 696–718 (1998).
[79] F. Murat, *Compacité par compensation.* Ann. Scuola Norm. Sup. Pisa Sci. Fis. Mat **IV**, 489–507 (1978).
[80] P. Pedregal, *Relaxation in ferromagnetism: the rigid case*, J. Nonlin. Sci. **4**, pp. 105–125 (1994).
[81] P. Pedregal, *Parametrized Measures and Variational Principles*, Birkhäuser, Basel (1997).
[82] P. Pedregal, *Numerical computation of parametrized measures*, Num. Funct. Anal. Opt. **16**, pp. 1049–1066 (1995).
[83] F. Pistella, V. Valente, *Numerical stability of a discrete model in the dynamics of ferromagnetic bodies*, Num. Meth. PDEs **15** (1999).
[84] P. Podio-Guidugli, V. Valente, *Existence of global-in-time weak solutions to a modified Gilbert equation*, Nonl. Analysis **47**, pp. 147–158 (2001).
[85] P. Podio-Guidugli, G. Tomassetti, *On the evolution of domain walls in hard ferromagnets*, SIAM J. Appl. Math. **64**, pp. 1887–1906 (2004).
[86] N. Popović, D. Praetorius, *Application of $\mathcal{H}$-matrices in micromagnetics*, Computing (to appear).
[87] I. Privorotskii, *Thermodynamic theory of domain structures*, New York, Wiley (1976).
[88] A. Prohl, *Computational Micromagnetism*, Teubner, Stuttgart (2001).
[89] T. Roubíček, *Relaxation in Optimization Theory and Variational Calculus*, W. de Gruyter, Berlin (1997).
[90] T. Roubíček, M. Kružík, *Microstructure evolution model in micromagnetics*, Zeitschrift f. Angew. Math. Phys. **55**, pp. 159–182 (2004).
[91] T. Roubíček, M. Kružík, *Mesoscopic model for ferromagnets with isotropic hardening*, Zeitschrift f. Angew. Math. Phys., (to appear).
[92] M. Struwe, *Geometric evolution problems*, IAS/Park City math. Series **2**, pp. 259–339 (1996).
[93] P.L. Sulem, C. Sulem, C. Bardos, *On the continuous limit for a system of classical spins*, Comm. Math. Phys. **107**, pp. 431–454 (1986)
[94] J. Sun, F. Collino, P.B. Monk, L. Wang, *An eddy-current and micromagnetism model with applications to disk write heads*, Int. J. Numer. Meth. Engrg. **60**, pp. 1673–1698 (2004).
[95] L. Tartar, *Compensated compactness and applications to partial differential equations* . In: Nonlin. Anal. Mech. Herriot-Watt Symposium **IV** (R. Knops ed.) Pitman Res. Notes Math. **39** 136–212 (1979).
[96] C. Truesdell, W. Noll, *The nonlinear field theories in mechanics.* In: Encyclopedia of Physics, **III/3**, Springer, Heidelberg, 1965.
[97] A. Visintin, *On Landau-Lifshitz' equations for ferromagnetism*, Japan J. Appl. Math. **2**, pp. 49-84 (1985).
[98] A. Visintin, *Differential models of hysteresis*, Springer, Berlin, (1994).
[99] A. Visintin, *Modified Landau-Lifshitz equation for ferromagnetism*, Physica B **233**, pp. 365–369 (1997).
[100] L.R. Walker, *A treatise on magnetism, vol. III*, G.T. Rado & H. Suhl (eds), Academic Press, New York, pp. 450–453 (1963).

[101] X.-P. Wang, C.J. García-Cervera, W. E, *A Gauss-Seidel projection method for micromagnetics simulations*, J. Comp. Phys. **171**, pp. 357–372 (2001).

[102] L.C. Young, *Generalized curves and existence of an attained absolute minimum in the calculus of variations*, Comptes Rendus de la Société et des Lettres de Varsovie, Classe **III 30**, pp. 212–234 (1937).

Institute of Information Theory and Automation, Academy of Sciences of the Czech Republic, Pod vodárenskou věží 4, CZ-182 08 Praha 8, Czech Republic

E-mail address: kruzik@utia.cas.cz

Department of Mathematics, ETHZ, CH-8092 Zurich, Switzerland

E-mail address: apr@math.ethz.ch